Review Article

Shrinking and Elastic Properties of Coniferous Wood in Relation to Cellular Structure*[1]

Ugai WATANABE*[2]

(Received June 1, 1998)

Keywords: shrinkage, shrinkage anisotropy, Young's modulus, specific Young's modulus, power spectrum analysis, cell model

Contents

*[1] This review article is the abstract of the doctor thesis by the author (Kyoto University, 1998).

*[2] Laboratory of Property Enhancement.

General Introduction

Wood is a cellular solid and at the same time a composite material. A composite material contains one or more types of discrete units which are arranged in a regular repetitive pattern or whose distribution is random or graded. On the other hand, a cellular solid is an assembly of cells with solid edges or faces, packed together so that they fill space. Wood is generally composed of layers of early wood and late wood made up of highly elongated cells in the longitudinal direction. The cell walls are composed of multi-layers, that is, the intercellular layer, the primary wall and the secondary walls. In each layer, cellulose molecules are grouped together in long filaments called microfibrils embedded in a matrix composed of amorphous hemicelluloses and lignin. The excellent characteristics in the physical and mechanical properties of wood result from these structures ranging from macroscopic to microscopic and molecular levels.

It is essential that the structural characteristics of wood as both a cellular solid and a composite material are taken into consideration to investigate its physical and mechanical properties. However, it is very difficult to evaluate quantitatively the structural characteristics of wood, particularly, transverse cell shapes, size and arrangement, because there is a wide distribution in its structures.

With recent advances of computer technology, image analyzing techniques have been remarkably developed. Among several techniques, the analysis of the power spectrum obtained by two dimensional fast Fourier transform has been adopted to identify the morphological features of wood cells. This analyzing technique was considered to be applicable for the quantitative evaluation of the transverse cell shape, size and arrangement. Therefore, it was suggested that this technique was useful to analyze the relationship between the structure and properties of wood in the transverse direction.

This article deals with the shrinkage and elasticity in relation to structures for coniferous woods. In Chapter 1, the relationships among the shrinkage, the Young's modulus and the specific gravity for the normal and compression woods of several conifers in the three principal directions are discussed. In Chapter 2, the effects of the cellular and layered structures on the shrinkage deformation of several coniferous wood cells in the radial and tangential directions are examined using the replica method and power spectrum analysis. In Chapter 3, the shrinkage anisotropy on the transverse plane is analyzed using a two layered model. In Chapter 4, the effects of the transverse cell shape on the tangential Young's modulus of early wood are examined through theoretical analysis on the cell models.

Chapter 1. Shrinkage and Elasticity of Normal and Compression Woods in Conifers

1.1 Introduction

It is generally recognized that the shrinkage of wood in the transverse direction increases with increasing its specific gravity. In coniferous woods, however, specific gravity distributes within a relatively narrow range and cell shapes in early wood vary among species, so that it is uncertain that there is a clear correlation between the shrinkage and the specific gravity, especially for compression wood. It has been also suggested that elastic deformation is closely related to shrinkage deformation. However, there are only a few reports which have dealt with this issue.

The growing stock of useful tropical hardwoods has decreased and the timber supply from these woods is uncertain. Tropical coniferous woods, such as *Agathis bornensis* Warb. and *Podocarpus imbricatus* Bl., are expected as substitutes for useful tropical hardwoods because of the abundant stock of natural growing trees with a large diameter. However, a large amount of compression wood is irregularly distributed throughout their trunks, which

causes serious warp and distortion of the lumber during sawing and drying and reduces their usefulness. If the differences in shrinkage and Young's modulus between normal and compression woods can be totally determined, the extent of warp and distortion of the lumber during processing can be estimated and reduced by proper log bucking and heat treatment.

In this chapter, the relationships among the specific gravities, shrinkages and Young's moduli for five coniferous woods including *A. bornensis* and *P. imbricatus* were investigated in relation to wood structure. Furthermore, the anatomical structures of *A. bornensis* and *P. imbricatus* were observed for the lack of their information.

1.2 Materials and Method

1.2.1. Wood specimens

Normal and compression woods of *Agathis bornensis* Warb., *Podocarpus imbricatus* Bl., *Cryptomeria japonica* D. Don, *Chamaecyparis obtusa* Endl., and *Picea sitchensis* Carr. were used for this experiment. Their specific gravities are shown in Table 1. The compression wood samples in *A. bornensis* and *P. imbricatus* were distinguished from the normal ones by their darker colors.

1.2.2. Measurements of shrinkages and specific gravity

Thirty specimens of 5 mm (radial) by 5 mm (tangential) by 100 mm (longitudinal) were prepared from the normal and compression wood samples of each species. Thus, the total number of specimens was 300. To measure the longitudinal shrinkage, a center line along the grain on the radial surface of the specimens was drawn with water proof and fade proof pigment ink. In the same way, to measure the radial and tangential shrinkages, a center line was drawn on the edge and flat-sawn grain surfaces of the specimens perpendicular to the grain, respectively. All of the specimens were soaked in distilled water under vacuum until fully saturated. The dimensions of the water saturated specimens in three directions were measured to the nearest 0.01 mm using a digital sliding caliper. After the measurements, the specimens were left under room condition for a few days, then placed in a closed chamber at 98% R.H. for five days. After conditioning, the specimens were dried over *di*-phosphorus pentaoxide under vacuum at 60°C, followed by drying overnight at 105°C. Finally, the dimensions and weights of the specimens in the oven-dried condition were measured to determine the specific gravity as well as the shrinkages from green to oven dry. These drying processes were adopted in order to avoid the collapse of the specimens.

1.2.3. Measurements of Young's moduli

After the measurements of shrinkages, the Young's moduli in the longitudinal, radial, and tangential directions for the same specimens were obtained. In the longitudinal direction, a three-point bending test (head speed : 1 mm/min.) below the proportional limit was conducted at room temperature. During the test, the specimens were loosely lapped by

thin polyvinylidene chloride film to keep them in the oven-dried condition. The specimens of 5 mm (radial) by 5 mm (tangential) by 10 mm (longitudinal) for the transverse compression tests were cut from the central portion of the specimens used for the bending test. The compression tests (head speed: 1 mm/min.) for the oven-dried specimens were performed at room temperature. The displacement of cross head was regarded as that of specimen by compressive load, so that the Young's moduli obtained by this experiment were apparent Young's moduli.

1.2.4. Microscopic observations

Observations using light and scanning electron microscopes (LM, SEM) were conducted to confirm whether the darkly colored specimens of *A. bornensis* and *P. imbricatus* consisted of compression wood or not. The small wood blocks were subjected to sliding-microtomy after softening in boiling water to take 20 μm thick sections. Sections mounted in biolite after safranine staining were subjected to LM observation. The remaining blocks, after microtoming, were dried slowly to the oven-dried condition to avoid the collapse. Then, they were ion-sputter-coated with Au for SEM observation (HITACHI S-500).

1.3. Results and Discussion

1.3.1. Structure of Agathis bornensis and Podocarpus imbricatus

A. bornensis and *P. imbricatus* are tropical conifers, which belong to Araucariaceae and Podocarpaceae, respectively. The crown of *A. bornensis,* although it is a coniferous wood, is similar to that of hardwood. *A. bornensis* has a comparatively large amount of stem-formed wood and few knots. *P. imbricatus* has a relatively large and straight trunk with few knots.

Fig. 1.1 shows the radial surfaces of woods of *A. bornensis* and *P. imbricatus*. No distinct growth rings were discerned in either of the woods. The heartwood of *P. imbricatus* is yellowish white and the sapwood is creamy white. The texture of *P. imbricatus* is fine and the grain is straight. In *A. bornensis,* on the other hand, there is no distinct differentiation between heartwood and sapwood. The wood is brown to pinkish brown. The texture is moderately fine and the grain is straight.

The darkly colored portions indicated by arrows in Fig. 1.1 are commonly called compression wood in timber industry. As shown in Fig. 1.2, they are randomly distributed all over the transverse surface of the stem. Therefore, almost all timbers from *A. bornensis* and *P. imbricatus* include compression wood. Generally, it is considered that compression wood is formed on the underside of inclined stems and branches[1]. However, the compression wood in *A. bornensis* and *P. imbricatus* was irregularly distributed even in the straight stems. The compression wood distribution in these species was remarkably different from that of temperate coniferous woods such as *C. japonica, C. obtusa,* and *P. sitchensis.*

Table 1.1 shows the mean values of volumetric shrinkage as well as three directional

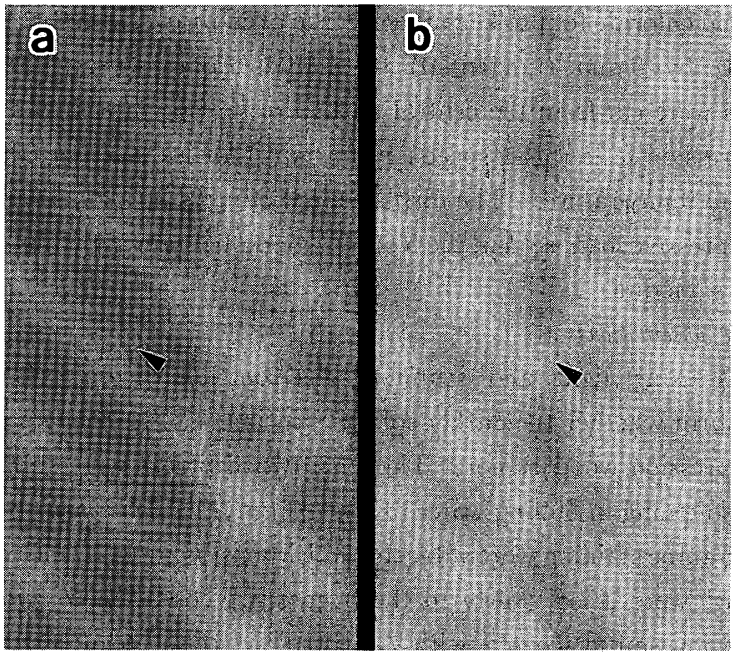

Fig. 1.1. Radial surfaces of *Agathis bornensis* (a) and *Podocarpus imbricates* (b). The darkly colored wood portions (arrow heads) are called compression wood in timber industry.

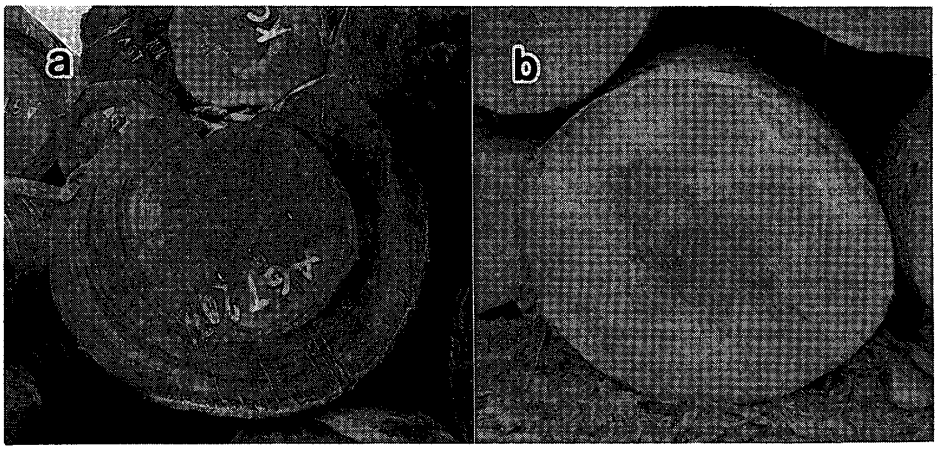

Fig. 1.2. Transverse surfaces of the stems of *Agathis bornensis* (a) and *Podocarpus imbricatus* (b).

shrinkages from the green to the oven-dried condition for all of the specimens examined. The shrinkage decreased in the order of tangential, radial, and longitudinal directions. The longitudinal shrinkage of compression wood was larger than that of normal wood. On the other hand, the radial and tangential shrinkages of normal wood were larger than those of compression wood except in the radial direction of wood for *P. imbricatus*.

Fig. 1.3 shows the results of LM and SEM observations of the darkly colored specimens for *P. imbricatus*. Some specimens had the features of compression wood, that is, the

Table 1.1. Mean values of specific gravities and three directional shrinkages for five species.

Species	Specific gravity	Shrinkage (%)				T/R ratio
		Vol.	L	R	T	
Cryptomeria japonica						
Normal	0.32	9.0	0.23	2.2	6.4	3.2
Compression	0.43	6.2	0.94	1.8	3.6	2.0
Chamaecyparis obtusa						
Normal	0.43	8.7	0.21	3.7	6.7	1.8
Compression	0.56	7.2	0.92	2.8	5.1	1.8
Picea sitchensis						
Normal	0.48	12.2	0.25	4.7	7.6	1.6
Compression	0.48	7.6	0.58	2.4	4.5	1.9
Agathis bornensis						
Normal	0.52	13.4	0.27	5.0	8.3	1.7
Compression	0.58	8.8	1.04	2.6	5.1	2.0
Podocarpus imbricatus						
Normal	0.36	11.3	0.24	2.8	8.6	3.1
Compression	0.52	12.5	0.64	4.3	7.7	1.8

Note: L: longitudinal direction, R: radial direction, T: tangential direction, Vol.: volume.

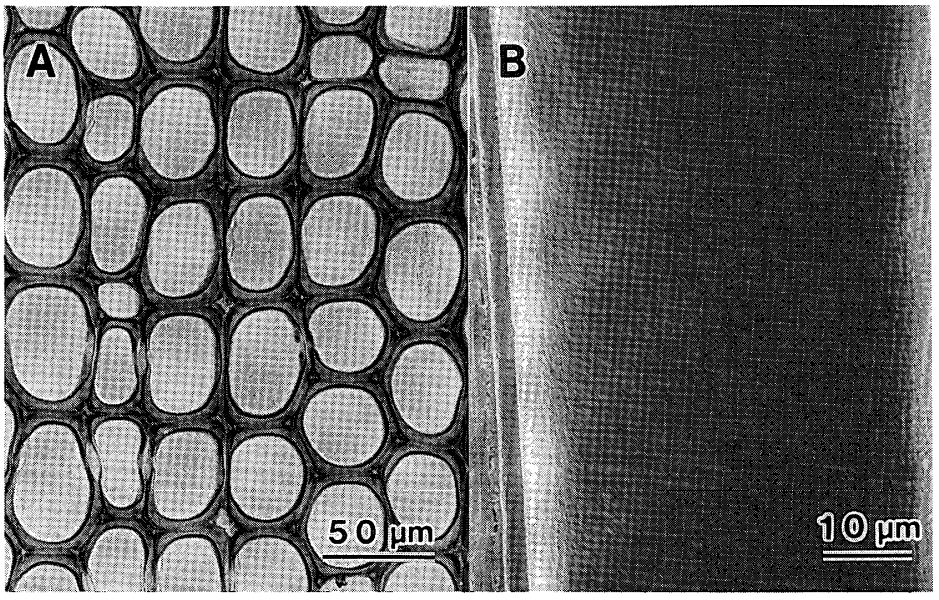

Fig. 1.3. Micrographs of the darkly colored wood portion of *Podocarpus imbricatus*. A: LM photograph of moderately thicker cell walls. B: SEM photograph of the S_3 layer with flat orientation of microfibrils.

tracheids had thicker cell walls and helical checks, and had no S_3 layer. However, the tracheids of other specimens in *P. imbricatus* had the S_3 layer and lacked helical checks, although they had moderately thicker cell walls. These observations suggested that the

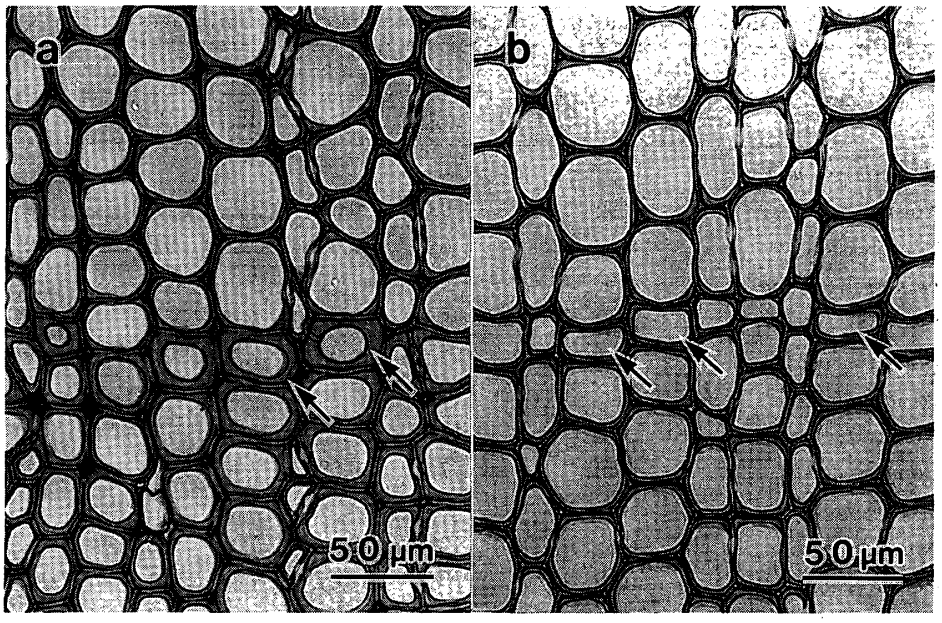

Fig. 1.4. Transverse sections of *Agathis bornensis* (a) and *Podocarpus imbricatus* (b). A small number of tracheids have relatively thicker walls and smaller radial diameters (arrows).

darkly colored portions were not always typical compression woods because they had structures similar to those of the normal wood portions. On the contrary, tracheids in the darkly colored portions of the specimens in *A. bornensis* showed the typical features of compression wood.

It is postulated[4] that one of the main causes of anisotropic shrinkage on the transverse plane is due to the difference in shrinkage between early and late woods. Fig. 1.4 shows micrographs of transverse sections of normal wood of *A. bornensis* and *P. imbricatus*. Although some tracheids had relatively thicker walls and smaller radial diameters, there were few late wood tracheids as defined by Mork[5]. It was noted that the woods of *A. bornensis* and *P. imbricatus* without distinct growth rings exhibited anisotropic shrinkage on the transverse plane, as shown in Table 1.1. These facts suggested that the anisotropic shrinkage on the transverse plane for these species did not result from the different shrinkages between early and late woods but depended on the cell shape, cell arrangement, and anisotropic structure in the cell wall.

1.3.2. Relationship between shrinkage and specific gravity

Fig. 1.5 shows the relationships between the longitudinal shrinkages S_L and the specific gravities γ of all of the specimens examined. In the figure, open and closed symbols represent the normal and compression woods, respectively. There was no definite correlation between S_L and γ for the normal wood, as S_L were about 0.2 to 0.3% regardless of γ. On the other hand, in the higher range of γ of compression wood, S_L increased mostly with increasing γ for each wood species. As the extent of compression wood increases, the

specific gravity and mean microfibril angle increase. It is generally accepted that compression wood compared to normal wood has a larger mean microfibril angle, namely about in the S_2 layer of the cell wall[6]. Furthermore, there are a few papers[7,8] reporting that the microfibril angle does not always indicate the extent of compression wood. However, the increase in longitudinal shrinkage with increasing specific gravity suggested that the extent of compression wood probably depends on the mean microfibril angle.

Fig. 1.6 shows the relationships between the radial shrinkages and the specific gravities γ of all of the specimens examined. It seemed that of the normal wood generally increased with increasing γ (r=0.864). However, when examined for each species, S_R varied widely within a narrow range of γ. On the other hand, for compression wood, there was no clear correlation between S_R and γ, not only for each species, but for all species. Wood has a comparatively regular cell arrangement in series in the radial direction, so it is probable that the increase in specific gravity increases the radial shrinkage. The results did not always show this trend. Thus, the cell shape may affect the radial shrinkage to some extent.

Fig. 1.7 shows the relationships between the tangential shrinkages S_T and the specific

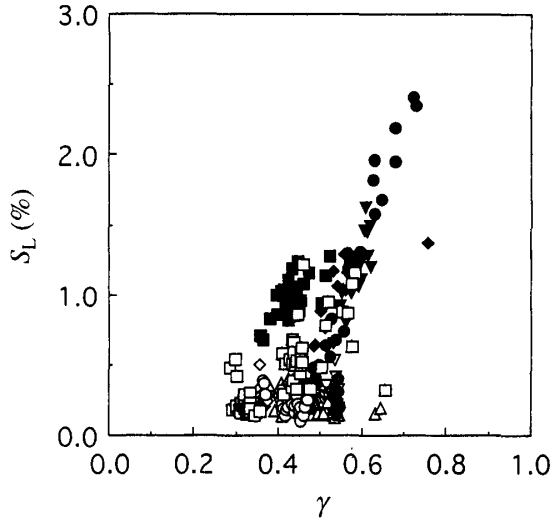

Fig. 1.5. Relationships between specific gravities (γ) and longitudinal shrinkages (S_L) for all of the specimens examined. Legends: □ and ■: normal and compression woods of *Cryptomeria japonica*, ○ and ●: normal and compression woods of *Chamaecyparis obtusa*, △ and ▲: normal and compression woods of *Picea sitchensis*, ▽ and ▼: normal and compression woods of *Agathis bornensis*, ◇ and ◆: normal and compression woods of *Podocarpus imbricatus*.

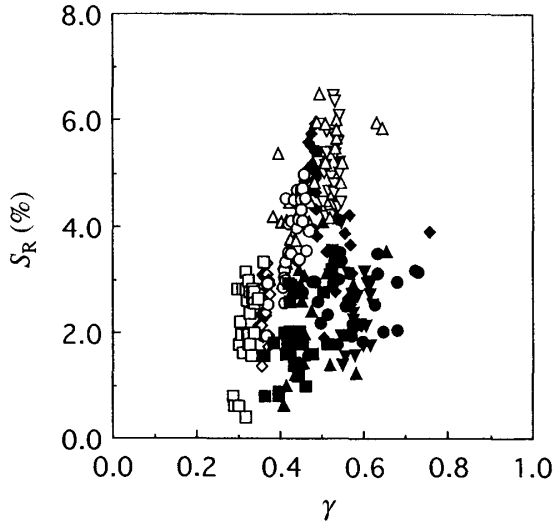

Fig. 1.6. Relationships between specific gravities (γ) and radial shrinkages (S_R) for all of the specimens examined. Legends: Refer to Fig. 1.5.

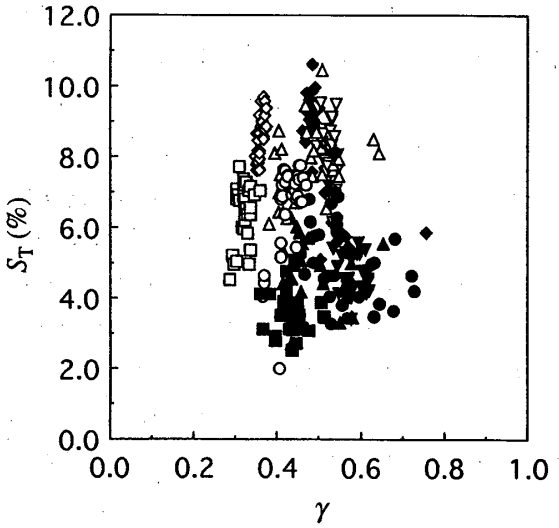

Fig. 1.7. Relationships between specific gravities (γ) and tangential shrinkages (S_T) for all of the specimens examined. Legends: Refer to Fig. 1.5.

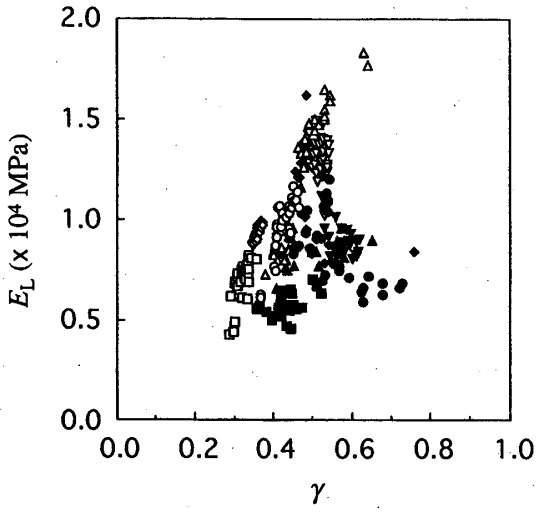

Fig. 1.8. Relationships between specific gravities (γ) and longitudinal Young's modulus (E_L) for all of the specimens examined. Legends: Refer to Fig. 1.5.

gravities γ of all of the specimens examined. No correlation was detected between them, as in the case of S_R. However, S_T was certainly larger than S_R regardless of wood species when compared at the same γ. In general, the cell arrangement in the tangential direction is much more irregular than that in the radial direction, and the modes of cell arrangement are different among wood species. However, this fact is not considered to relate to the anisotropic shrinkage on the transverse plane.

There was, therefore, no clear correlation between the volumetric shrinkages and the specific gravities for all of the specimens of the normal and compression woods.

1.3.3. Relationship between Young's modulus and specific gravity

Fig. 1.8 shows the relationships between the specific gravities γ and the longitudinal Young's moduli E_L obtained by the bending test for all of the specimens. E_L of normal wood increased with increasing γ. Contrary, there was no correlation between γ and E_L for compression wood. Nevertheless compression wood showed higher γ, E_L of compression wood was smaller than that of normal wood. This result is attributed to larger microfibril angles of compression wood tracheids, as in the case of S_L.

Fig. 1.9 shows the relationships between the specific gravities γ and the Young's moduli in the radial and tangential directions, E_R and E_T, which were obtained by the compression test for all of the specimens. E_R and E_T increased with increasing γ. E_R and E_T varied widely within a narrow range of γ, although a correlation was observed between γ and E_R or E_T. γ varied also widely within a narrow range of E_R or E_T. This fact was considered to be due to the differences in cell shapes on the transverse plane.

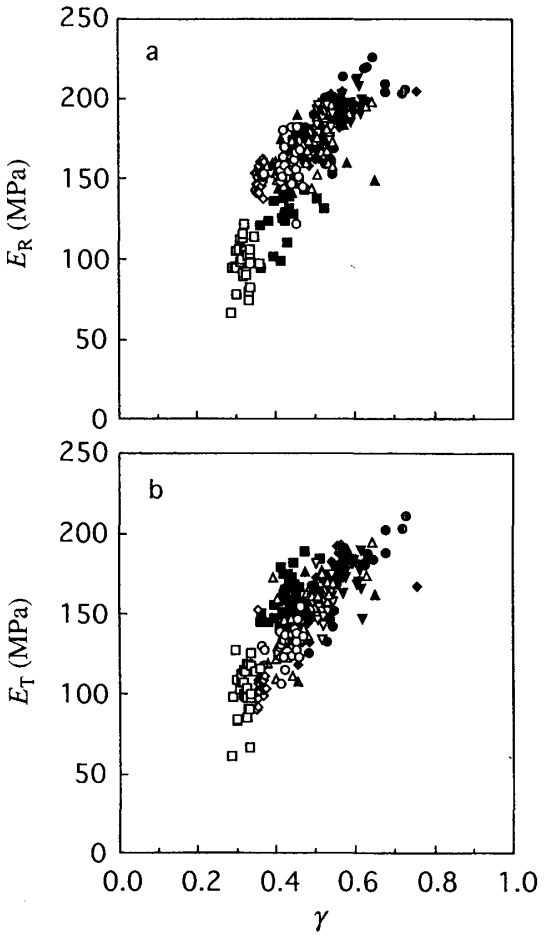

Fig. 1.9. Relationships between specific gravity (γ) and Young's moduli (E_R, E_T) in both the radial (a) and the tangential (b) directions for all of the specimens examined. Legends: Refer to Fig. 1.5.

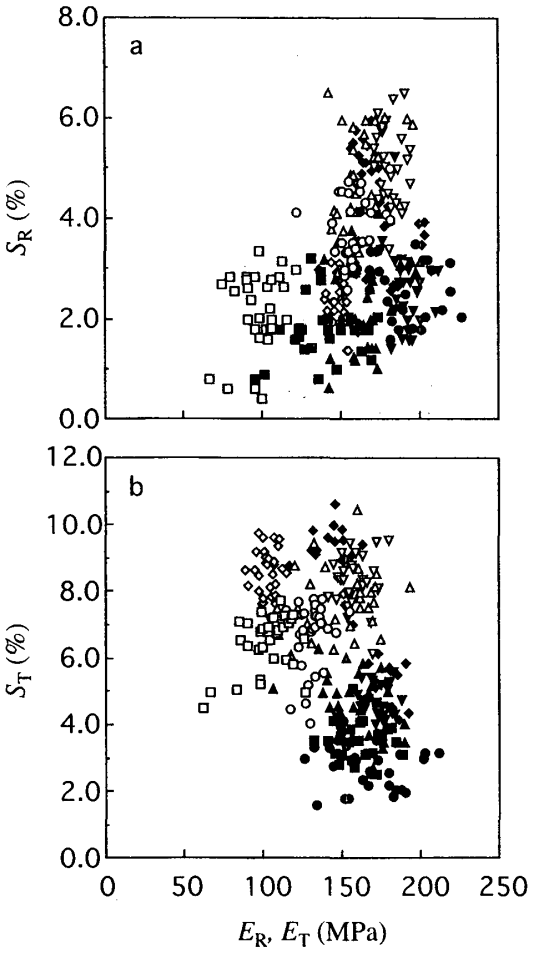

Fig. 1.10. Relationships between Young's moduli (E_R, E_T) and shrinkages (S_R, S_T) in both the radial (a) and the tangential (b) directions for all of the specimens examined. Legends: Refer to Fig. 1.5.

1.3.4. Relationship between shrinkage and Young's modulus

Fig. 1.10 shows the relationships between the shrinkages and the Young's moduli in the radial and tangential directions. No clear correlation was observed between the shrinkages and the moduli except for the result in the radial direction of normal wood. The shrinkage seemed to increase with increasing Young's modulus for normal wood in the radial direction. The linear correlation coefficient was 0.684.

On the other hand, in the longitudinal direction, there was a correlation between the shrinkage S_L and the Young's modulus E_L. S_L decreased with increasing E_L. However, S_L of compression wood was larger than that of normal wood when compared at the same E_L. When S_L was plotted against the specific Young's modulus (the Young's modulus divided by the specific gravity, E_L/γ), there was a good correlation between them for both

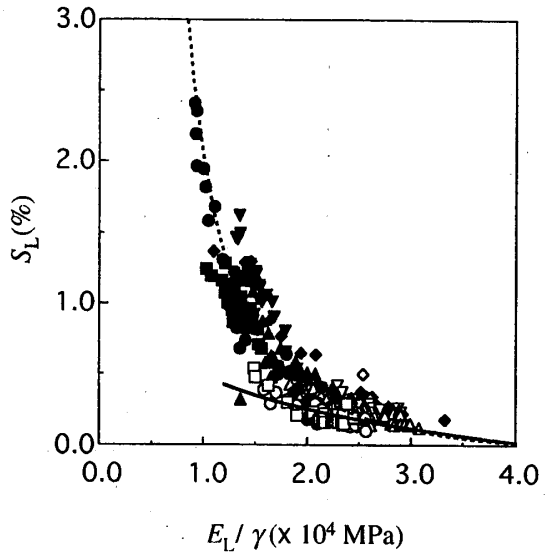

Fig. 1.11. Relationship between specific Young's moduli (E_L/γ) and shrinkages (S_L) in the longitudinal direction for all of the specimens examined. Solid and dashed lines show Equation (1-3) for normal and compression wood specimens, respectively. Legends: Refer to Fig. 1.5.

normal and compression woods, as shown in Fig. 1.11. Even in this case, S_L of normal wood was smaller than that of compression wood when compared at the same E_L/γ.

The above result can be explained as follows. Almost all cells of coniferous wood are tracheids. Therefore, using a parallel multilayer model composed of cell walls and air, the longitudinal Young's modulus E_L of coniferous wood, as a first approximation, can be expressed by the following law of mixtures.

$$E_L = \Sigma(\delta_{wi}E_{Lwi} + \delta_{ai}E_{ai}) \cong \Sigma \delta_{wi}E_{Lwi}, \quad \Sigma(\delta_{wi} + \delta_{ai}) = 1, \tag{1-1}$$

where E_{Lwi} and δ_{wi} are the longitudinal Young's modulus and the volume fraction of the i-th wall layer, respectively, while E_{ai} ($\cong 0$) and δ_{ai} are those of the i-th air layer. The specific gravity γ is given by $\gamma = \Sigma \delta_{wi}\gamma_{wi}$, where γ_{wi} is the specific gravity of the i-th wall layer. When the mean specific gravity γ_w and the mean longitudinal Young's modulus of the cell wall E_{Lw} are defined by $\gamma/\Sigma\delta_{wi}$ and $\Sigma\delta_{wi}E_{Lwi}/\Sigma\delta_{wi}$, respectively, E_{Lw} is given by

$$E_{Lw} = E_L(\gamma_w/\gamma) \tag{1-2}$$

The mean specific gravity γ_w can be regarded as a constant value of 1.45 in the oven-dried condition irrespective of wood species, so that E_L/γ is proportional to E_{Lw}. In the same way, when the longitudinal shrinkage from the wet condition to the oven-dried condition of the i-th wall layer is denoted by S_{Lwi} and the mean longitudinal shrinkage of the cell wall S_{Lw} is defined by $\Sigma\delta_{wi}S_{Lwi}/\Sigma\delta_{wi}$, the longitudinal shrinkage of wood S_L corresponds to S_{Lw}. These results indicate that E_L/γ, instead of E_L, should be related to S_L to examine the relationship between E_{Lw} and S_{Lw} in the longitudinal direction.

Assuming that at zero mean microfibril angle S_L is zero and $E_L/\gamma=4.25\times10^4$ MPa ($E_{Lw}=6.16\times10^4$ MPa), the relationship between E_L/γ (MPa) and S_L (%) was described by the following empirical equation:

$$S_L=-C+\frac{b}{(E_L/\gamma)^a}, \tag{1-3}$$

where $C=b\,(\gamma_w/E_0)^a$, $a=8.66\times10^{-3}$ and $b=42.4$ for normal wood specimens, and a=2.15 and b=8.21×10^8 for compression wood specimens. The mean microfibril angle θ greatly affects to both and in the longitudinal direction[9,10]. Therefore, it is considered that E_{Lw} is closely related to S_{Lw} through θ.

The following expression between E_{Lw} and θ has been proposed for normal wood[9].

$$E_{Lw}(\theta)=\frac{E_0}{1+k\theta^2}, \tag{1-4}$$

where k is a factor which depends on both temperature and moisture content. Combining Equations (1-2), (1-3), and (1-4) gives the prediction of the relationship between $S_L(\theta)$ and θ, expressed as follow:

$$S_L(\theta)=C\{(1+k\theta^2)^a-1\} \tag{1-5}$$

The value of k was calculated to be 0.00735. In Fig. 1.12, the calculated values of Equation (1-5) for normal wood specimens are compared to the experimental values obtained by Cockrell[10].

Barber and Meylan[11] analyzed theoretically the relationship between $S_L(\theta)$ and θ using a cell wall model in which long microfibrils of crystalline cellulose were embedded in a matrix of lignin and hemicelluloses. Furthermore, Barber[12] extended the model by adding a thin outer layer to Barber and Meylan's model. Cave[13] analyzed the relationship between $S_L(\theta)$ and θ using a model in which a Gaussian distribution of the microfibril angle was taken into account.

A theoretical curve obtained by using Barber and Meylan's model is shown in Fig. 1.12. This curve was obtained by using the values: 134 GPa for the elastic modulus of the microfibrils, 0.77 GPa for the modulus of rigidity of the matrix substance, and 1.66 GPa for the bulk elastic modulus of the matrix substance. Barber and Meylan's model predicted negative values of $S_L(\theta)$ when θ was between about 10° and 40°. The models by Barber and Cave also give rise to negative values in this range. However, the experimental values of $S_L(\theta)$ of normal wood increase with increasing θ. On the contrary, the predicted values for normal wood obtained from Equation (1-5) agreed reasonably well with the experimental values.

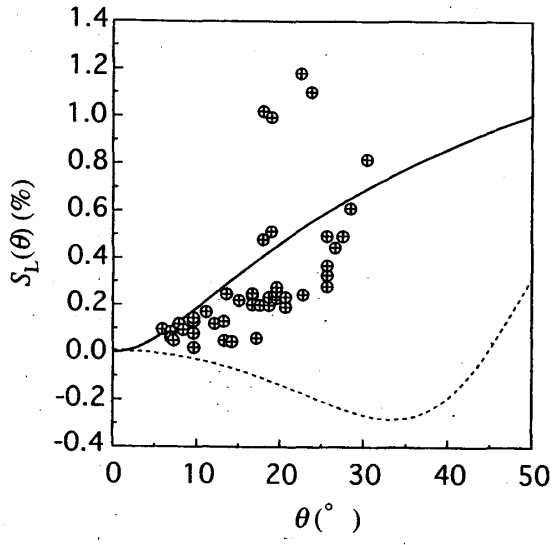

Fig. 1.12. Comparison of calculated values from Equation (1-5) for normal wood (solid line) to experimental values (⊕)[10] and theoretical values by Barber and Meylan's model (dashed line)[11].

Chapter 2. Transverse Shrinkage of Coniferous Wood Cells

2.1 Introduction

The anisotropic shrinkage of coniferous woods on the transverse plane has been considered to arise mainly from the difference in shrinkage between early wood and late wood. Pentoney[14] and Nakato *et al.*[15], however, reported that the separated early wood itself showed a transverse anisotropic shrinkage. The results obtained in Chapter 1 also suggest that the cellular structure greatly affects the shrinkage anisotropy on the transverse plane. From these results, the anisotropic shrinkage may be related to cell shape and arrangement as well as to the cell wall structure.

To investigate the shrinkage of wood at the microscopic level, thin wood sections have been used[16,17]. However, small cracks often occur during the preparation[18]. The shrinkage of a thin section does not always represent that of whole wood. On the other hand, the replica method wherein the surface of wood is replicated on a film softened by heating is suitable for tracing the real cell deformation of whole wood at the same position.

Furthermore, a statistical treatment is necessary to estimate the relationship between cell shape and anisotropic shrinkage on the transverse plane because there is a wide dispersion in cell shape and size. For this purpose, the analysis of the power spectrum obtained by two-dimensional fast Fourier transformation is considered to be one of the best methods. Two dimensional variations in constituent elements of an image are transformed into frequency components on the power spectrum. The periodicity and directionality of elements which specify the feature of an image can be estimated from the power spectrum

pattern. There is some periodical and directional cell arrangement in wood structure. From this information, a statistically most probable shape of wood cell can be constructed[19].

In this chapter, the replica method and power spectrum analysis were used to investigate the shrinkage behavior of several coniferous wood cells.

2.2. Materials and Methods

2.2.1. Wood specimens

The normal wood of four kinds of conifers (*Cryptomeria japonica* D. Don, *Chamaecyparis obtusa* Endl., *Picea sitchensis* Carr., *Agathis bornensis* Warb.) and the compression wood of two kinds of conifers (*C. japonica* and *C. obtusa*) were used. The specimen size was 5 mm (radial) by 5 mm (tangential) by 30 mm (longitudinal).

2.2.2. Replica of transverse surface of specimen

After the specimens were soaked in distilled water until saturated, their transverse surfaces were smoothed using a sliding microtome. The surfaces of the specimen except the surface to be replicated were sealed with a thin polyvinylidene chloride film to avoid water evaporation. The specimen was attached to the chuck of a testing machine. A glass slide with a polyethylene film (0.1 mm thickness) softened by heating at about 130°C was put on the mount supported by four screws to adjust its position. Then, the specimen was pushed on the film to obtain the replica[20], as shown in Fig. 2.1. After that, it was dried slowly at

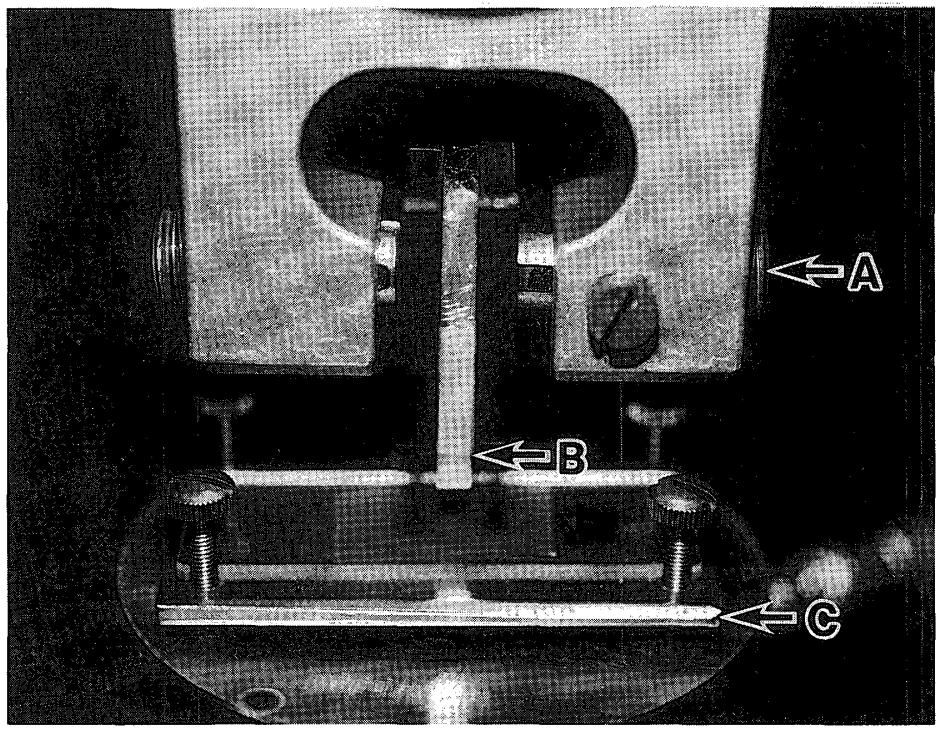

Fig. 2.1. Apparatus for the replica method. A: chuck of a testing machine, B: replicated specimens, C: mount for a glass slide with a softened film.

room temperature for five days, placed in a closed chamber conditioned at 98% R.H. for five days, dried over P_2O_5 at 60°C, then dried overnight at 105°C. A replica of the oven-dried specimen was also made in the same manner. The dimensions of specimens before and after drying were measured using a caliper to determine shrinkage.

2.2.3. Measurement of cell dimensions

The replicas obtained were observed under a light microscope and photographed. The figures of edges between walls and lumens on the photograph were traced onto a clear sheet and were input into an image analyzing system (Luzex III) using a TV camera. After the input images were smoothed and converted to the binary figures, the dimensions and areas of lumens as well as the thicknesses of the cell walls were measured on the monitor.

2.2.4. Power spectrum analysis

To investigate the effect of transverse cell shape on the shrinkage anisotropy in early wood, the replicas for the separated normal early wood of *C. obtusa* and *P. sitchensis* were subjected to the power spectrum analysis. Cell matrixes of 15 by 15 cells, set up on the photographs in the wet and oven-dried conditions, were traced onto clear sheets and were input into the image analyzing system. The input images were transformed to the binary images.

In order to determine the cell arrangement, the center of gravity for each cell was derived from the binary figures and was shown by a dot with diameter of 7 pixels on the monitor. A set of dots is mathematically expressed by the following function $D\ (s, t)$ which convolutes the delta functions of cell positions $\delta\ (s-x_i, t-y_i)$ and the aperture function of a dot $A\ (s, t)$[21].

$$D\ (s, t)=A\ (s, t) * \{\delta\ (s-x_1, t-y_1)+\cdots+\delta\ (s-x_N, t-y_N)\}, \qquad (2\text{-}1)$$

where x_i and y_i are coordinates of the i-th dot and * is an operator of convolution. After the dots and background were converted to the gray level image of 255 and 0, respectively, the two-dimensional fast Fourier transform (FFT) was conducted to obtain the power spectrum. The spectrum was saved on a floppy diskette and printed out. By the Fourier integration of $D\ (s, t)$, the power spectrum of the delta functions in polar coordinates (k, ϕ) is given by

$$P_\delta\ (k, \phi)=\frac{1}{2}\sum_{i=1}^{N}\sum_{j=1}^{N} 2\cos\frac{2\pi k\{(x_i-x_j)\cos\phi+(y_i-y_j)\sin\phi\}}{M}+N\ (i\neq j), \qquad (2\text{-}2)$$

where k is the frequency and M is the size of monitor (1,024 in this case).

The direction of cell arrangement can be estimated from the power spectrum density at each angle.

$$P_\delta\ (\phi)=\frac{1}{2}\sum_{i=1}^{N}\sum_{j=1}^{N}\int_{k_1}^{k_2}\left[2\cos\frac{2\pi k\{(x_i-x_j)\cos\phi+(y_i-y_j)\sin\phi\}}{M}+N\right]dk. \qquad (2\text{-}3)$$

The power density of each angle at a lower frequency band from 30 to 100 pixels was adapted to determine the direction of cell arrangement. The density was obtained by reading and integrating the gray levels of power spectrum image using a computer.

To investigate two dimensional orientation of the cell wall, the cell wall regions between adjacent lumens were painted by a computer, and a figure of the center line of the cell walls was made by thinning the thickness to one pixel. This figure was also converted to the gray level image and subjected to FFT to obtain the power spectrum which was saved on a floppy diskette.

The power spectrum of the image consisting of the rectangular elements with length L, width B and weight per unit area m is expressed by

$$P_r(k, \theta)=\frac{1}{\eta \bar{m}^2}\int_m\int_0^{2\pi} m^2 \sin c^2\{\pi kL \cos(\theta'-\theta)\} \cdot \sin c^2\{\pi kB \sin(\theta'-\theta)\} \cdot H(m, \theta')\, d\theta' dm, \quad (2\text{-}4)$$

where η and $\bar{m}$ are the number of elements and the weight per unit area of the image, and $H(m, \theta')$ is the function expressing the relationship between m and the longitudinal direction of an element θ[22]. The orientation of elements can be estimated by the power spectrum density at each angle.

$$p_r(\theta)=\int_{k_1}^{k_2} P_r(k, \theta)\, dk. \quad (2\text{-}5)$$

The following relationship is confirmed by a numerical analysis.

$$p_r(\theta+\pi/2)=\int_m H(m, \theta)\, dm. \quad (2\text{-}6)$$

The orientation of the cell wall was estimated by regarding the figure made by thinning the cell walls as consisting of rectangular elements. The power density of each angle at a higher frequency band from 200 to 300 pixels was adapted to determine the cell wall orientation. The density was obtained by reading and integrating the gray levels of the power spectrum image using a computer.

2.3. Results and Discussion

2.3.1. Shrinkage behavior of coniferous wood tracheids

As an example of normal wood, the transverse shapes of early wood tracheids in *C. obtusa* before (W) and after (D) drying are shown in Fig. 2.2A. The traced figure of the same tracheid indicated by asterisks in Fig. 2.2A is shown in Fig. 2.2B. The solid and dotted lines show the results in one typical cell before and after drying, respectively. The decrease in lumen diameter was 7.9% in the tangential direction and 1.5% in the radial direction. The shrinkages of the radial cell walls were 12.3% and 9.5%, while those of the tangential walls were 16.3% and 9.2%. The cell lumens of normal wood of *C. obtusa* shrank anisotropically by drying. The decrease in the tangential lumen diameter was larger than that in the radial diameter. Almost the same results were obtained for other species. In contrast, Fig. 2.3 shows the results of compression wood of *C. obtusa*. Lumens expanded and walls shrank after drying. The increase in lumen diameter was 12.5% in the tangential

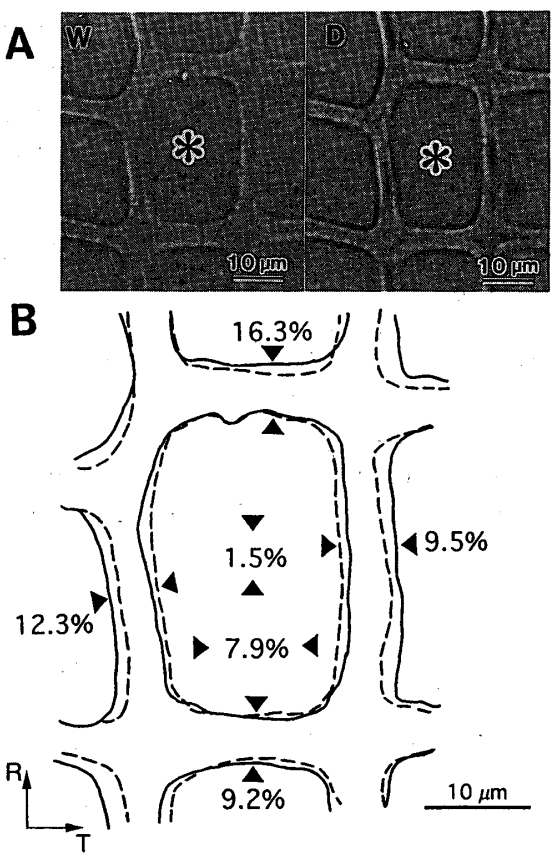

Fig. 2.2. Transverse shapes of early wood tracheids in normal wood of *Chamaecyparis obtusa*. A: replica photographs in wet (W) and oven-dried (D) conditions. B: traced figure of the tracheids in wet (solid line) and oven-dried (dotted line) conditions indicated by asterisks.

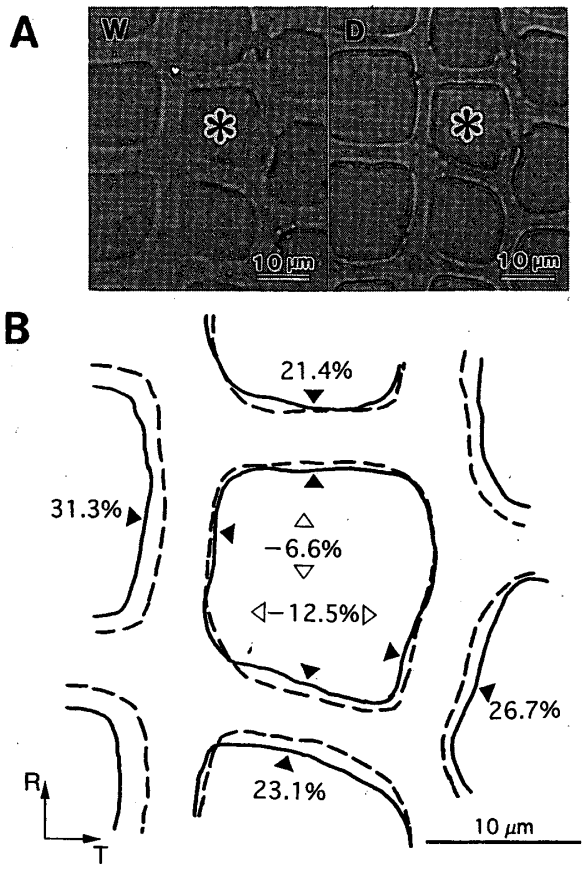

Fig. 2.3. Transverse shapes of compression wood tracheids of *Chamaecyparis obtusa*. A: replica photographs in wet (W) and oven-dried (D) conditions. B: traced figure of the tracheids in wet (solid line) and oven-dired (dotted line) conditions indicated by asterisks.

direction and 6.6% in the radial direction. The shrinkages of the radial walls were 26.7% and 31.3%, while those of the tangential walls were 21.4% and 23.1%. Almost the same results were obtained for *C. japonica*.

The histograms of the perimetric and areal changes in lumens for the normal and compression wood tracheids of *C. obtusa* are shown in Fig. 2.4. The results show that lumens shrank in normal wood and expanded in compression wood. This tendency was also recognized in other species. Table 2.1 shows the average values of the areal and perimetric changes in lumens for the normal and compression woods of four species. It has been considered that the cell lumen of wood remains almost unchanged during drying[23] and that the volumetric change of the wood is equivalent to the volume of water released from the cell wall. On the other hand, Chafe and Ilic[24] reported a lumen contraction during drying from green condition to 5% equilibrium moisture content. The results obtained suggested

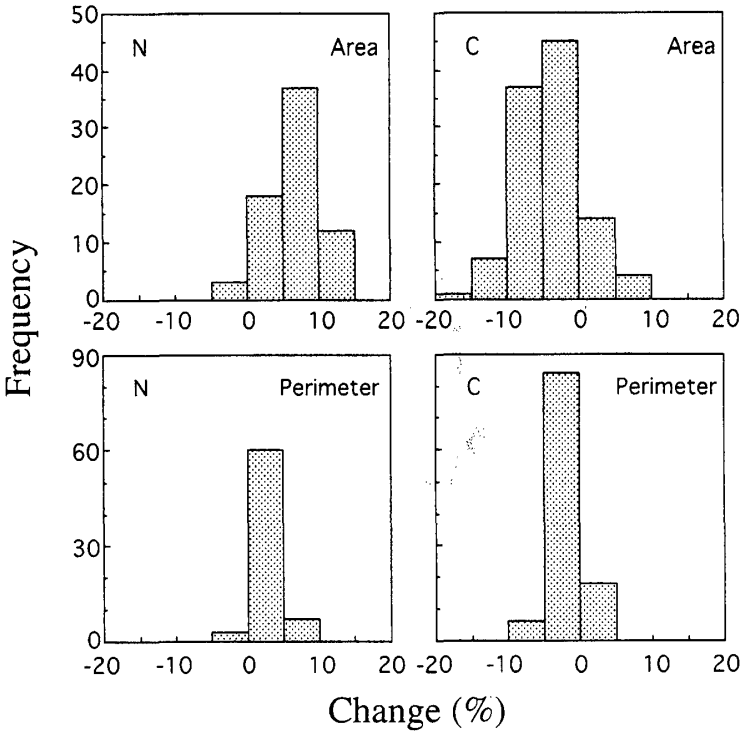

Fig. 2.4. Histograms for areal and perimetric changes in lumens of normal (N) and compression (C) woods ob *Chamaecyparis obtusa*. Positive values show shrinkage and negative values show expansion.

Table 2.1. Areal and perimetric decreases in lumens of four species examined. Positive values show shrinkage and negative values show expansion.

Species	Changes (%)	
	Area	Perimeter
Normal wood		
Cryptomeria japonica	6.8	2.7
Chamaecyparis obtusa	0.5	0.9
Picea sitchensis	13.8	6.4
Agathis bornensis	4.0	1.2
Compression wood		
Cryptomeria japonica	−3.8	−1.9
Chamaecyparis obtusa	−7.8	−4.3

Table 2.2. Mean values of radial (R) and tangential (T) cell wall shrinkages for four species examined.

Species	Shrinkage (%)	
	R	T
Normal wood		
Cryptomeria japonica	13.0	20.0
Chamaecyparis obtusa	11.5	13.3
Picea sitchensis	11.6	20.0
Agathis bornensis	15.1	16.1
Compression wood		
Cryptomeria japonica	18.3	21.4
Chamaecyparis obtusa	25.6	28.8

that the transverse shrinkage resulted not only from the shrinkage of the cell wall but also from a change in lumen size. Therefore, the change in lumen size must be also taken into consideration when analyzing the anisotropic shrinkage in wood.

Table 2.2 shows the average shrinkages of the radial and tangential walls in the

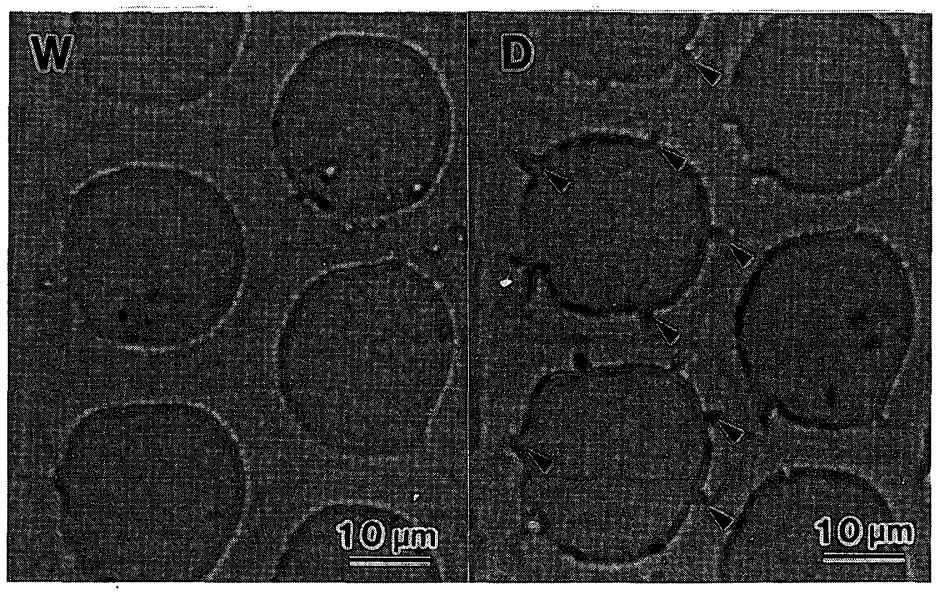

Fig. 2.5. Transverse shapes of compression wood tracheids of *Cryptomeria japonica*. W: wet condition, D: oven-dried condition. Helical checks were opened during drying (arrows).

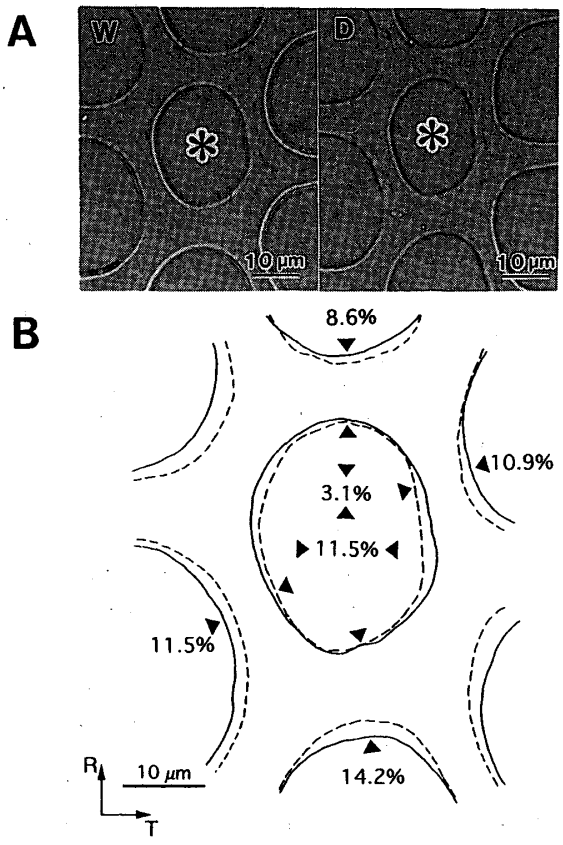

Fig. 2.6. Transverse shapes of tracheids of *Agathis bornensis*. A: replica photographs in wet (W) and oven-dried (D) conditions. B: traced figure of the tracheids in wet (solid line) and oven-dried (dotted line) conditions indicated by asterisks.

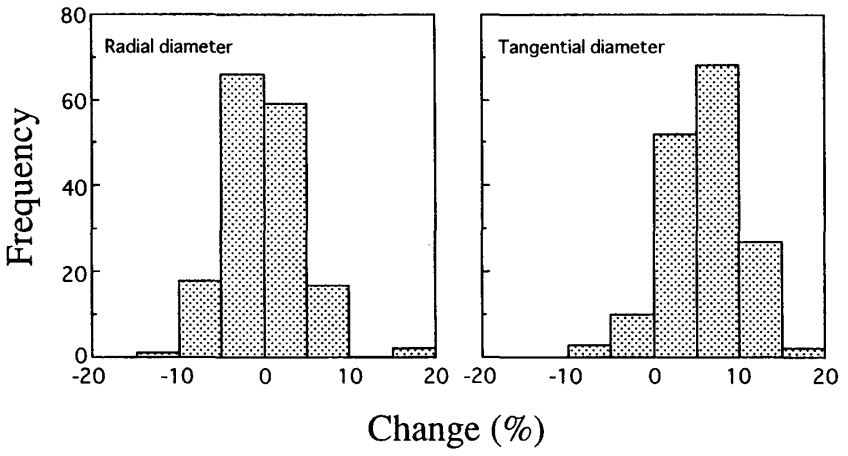

Fig. 2.7. Histograms for changes of radial and tangential lumen diameters of *Agathis bornensis*. Positive values show shrinkage and negative values show expansion.

thickness direction for the normal and compression woods. No distinct difference was recognized between the shrinkages of the radial and tangential walls except for the normal woods of *C. japonica* and *P. sitchensis*. The cell wall shrinkage in compression wood tracheid was much larger than that in normal wood tracheid, except for the tangential wall of *C. japonica* in which the former was slightly larger than the latter. The result indicates that in compression wood a higher extent of lignification is not always associated with a low shrinkage in the transverse direction.

It is considered that the difference in shrinkage behavior between the normal and compression wood tracheids depends on the differences in the cell wall structures. Normal wood tracheids have the S_3 layer, whereas compression wood tracheids lack it and have a thicker S_1 layer[6]. This thicker S_1 layer may restrain the shrinkage of other layers. Because the microfibrillar orientation in the S_3 layer is not entirely flat, the lumen areas of normal wood tracheids may be decreased during drying. Therefore, the shrinkage of a cell results from both the shrinkage of the cell wall and the change of the lumen. In the case of compression wood, the shrinkage of tracheids is restricted by the S_1 layer, nevertheless the cell wall has a higher shrinkage potential. This fact together with the absence of the S_3 layer results in the opening of helical checks. Fig. 2.5 shows the opening of helical checks and lumen expansion for the compression wood tracheids of *C. japonica*.

The anisotropic shrinkage on the transverse plane was also observed in *A. bornensis* which has no distinct growth rings; shown in Fig. 2.6. The macroscopic shrinkage in the tangential direction was larger than that in the radial direction. The lumen size reduced anisotropically. The decrease in lumen diameter was 11.5% in the tangential direction and 3.1% in the radial direction. The shrinkages of the radial walls were 10.9% and 11.5%, and those of the tangential walls were 8.6% and 14.2%. The histograms for the changes in

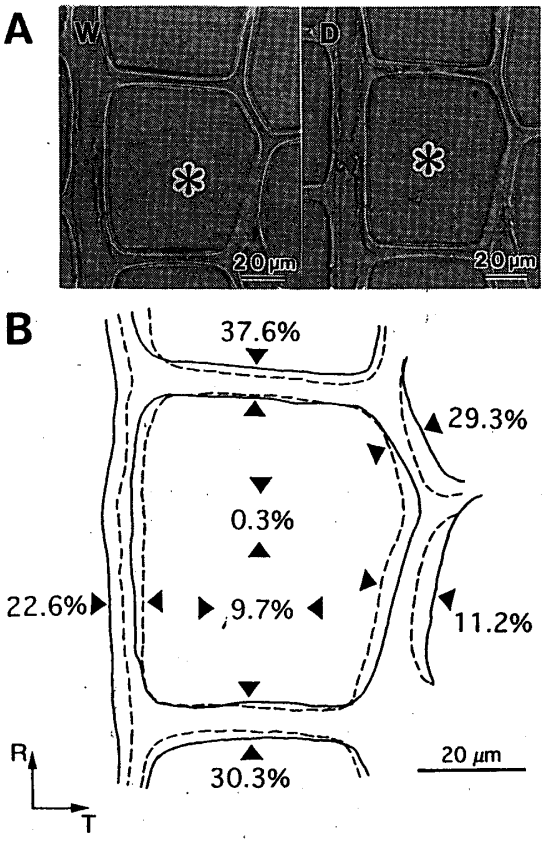

Fig. 2.8. Transverse shapes of early wood tracheids in normal wood of *Picea sitchensis*. A: replica photographs in wet (W) and oven-dried (D) conditions. B: traced figure of the tracheids in wet (solid line) and oven-dried (dotted line) conditions indicated by asterisks.

lumen diameter in the radial and tangential directions are shown in Fig. 2.7. The change in lumen diameter in the radial direction was distributed around 0%. On the other hand, almost all lumen diameters decreased in the tangential direction. This suggested that the strain restraint between early and late woods with different shrinkage potentials was not the only cause of anisotropic shrinkage in wood.

Fig. 2.8 shows the transverse shapes of early wood tracheids of *P. sitchensis* before and after drying. The decrease in lumen diameter was 9.7% in the tangential direction and 0.3% in the radial direction. The shrinkages of the radial walls were 11.2%, 22.6% and 29.3%, and those of the tangential walls were 30.3% and 37.6%. The change in included angle was recognized. These results suggested that the transverse shape of a cell greatly contributed to the anisotropic shrinkage in wood.

2.3.2. Cell shrinkage examined by power spectrum analysis

As an example, Fig. 2.9A and 2.9B show the center of gravity for each cell and the center line of the cell walls for *C. obtusa* under wet conditions. These figures are available for the estimation of cell wall orientation as well as the periodicity and direction of cell

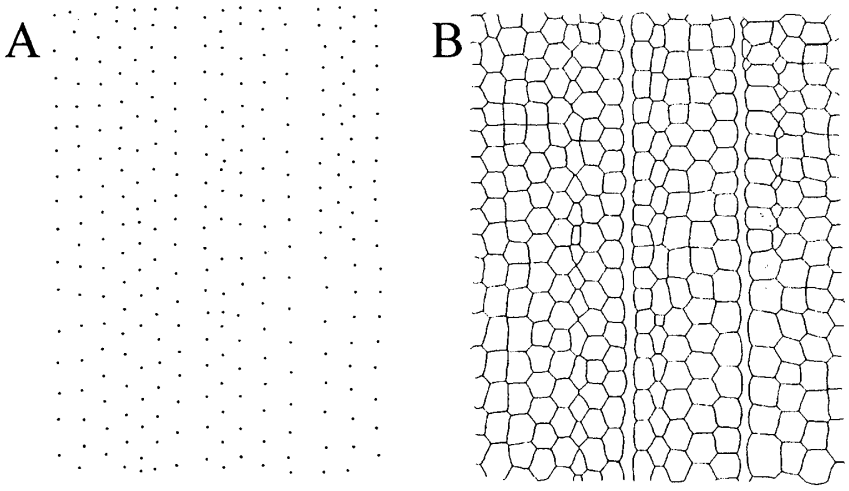

Fig. 2.9. Figures subjected to power spectrum analysis for *Chamaecyparis obtusa*. A: the center of gravity for each cell shown by a dot with diameter of 7 pixels. B: the center line of the cell walls.

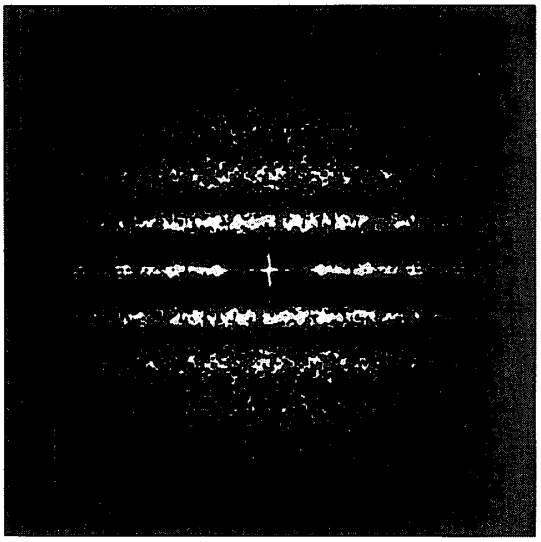

Fig. 2.10. Power spectrum obtained from the image shown in Fig. 2.9A.

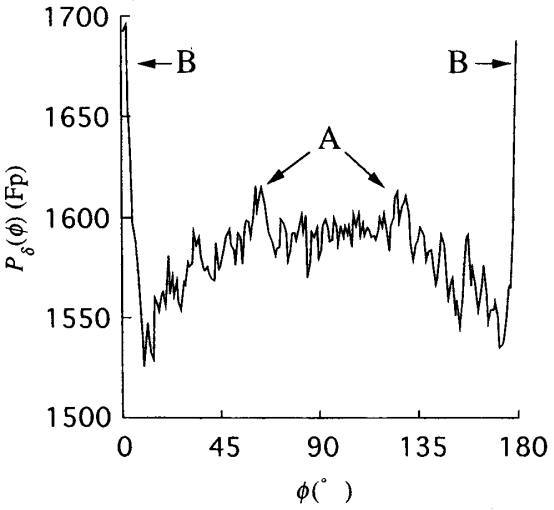

Fig. 2.11. $P_\delta(\phi)$ of *Chamaecyparis obtusa* in wet condition. Fp: floating points. Arrows A indicate the peaks related to the cell arrangement in the oblique direction, and arrows B those related to the radial files of tracheids.

arrangement.

Fig. 2.10 shows the power spectrum obtained from Fig. 2.9A. Equation (2-2) represents the Fourier transformation of all dots projected on a line in the ϕ direction. The periodicity of cell position in the radial direction ($\phi=\pi/2$) and the periodicity of radial files in the tangential direction ($\phi=0$) were determined from this equation. The direction of

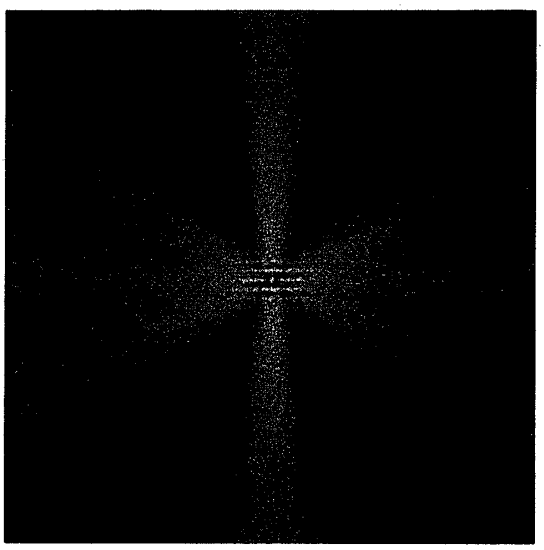

Fig. 2.12. Power spectrum obtained from the image shown in Fig. 2.9B.

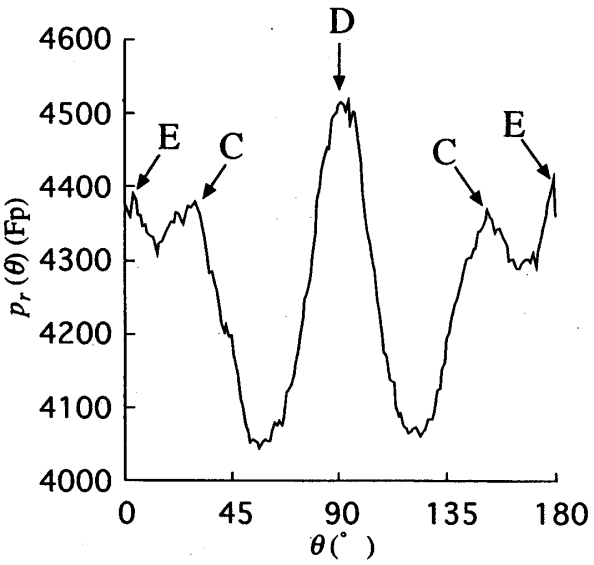

Fig. 2.13. $p_r(\phi)$ of *Chamaecyparis obtusa* in wet condition. Fp: floating points. Arrows C, D and E indicate the peaks related to the orientation of the radial cell walls, the tangential cell walls and ray tissues, respectively.

cell arrangement can be estimated from the power spectrum density at each angle. As the power with respect to a line passing (x_i, y_i) and (x_j, y_j) appears in the normal direction to the line, the direction of cell arrangement can be determined from the direction of strong power densities. Fig. 2.11 shows $P_\delta(\phi)$ of the spectrum shown in Fig. 2.10. Arrows A indicate the peaks related to the cell arrangement in the oblique direction, while arrows B indicate those related to the radial files of cells.

Fig. 2.12 shows the power spectrum obtained from Fig. 2.9B and Fig. 2.13 shows $p_r(\theta)$ of this spectrum. Arrows C and D indicate the peaks related to the orientation of the radial and the tangential cell walls. The peaks indicated by arrows E relate to the orientation of ray tissues. The orientation of the cell wall was determined from Equation (2-6).

The representative model of a transverse shape of tracheids was constructed by the following manner. Firstly, cell positions as shown in Fig. 2.14A were determined from the periodicities and directions of cell arrangement. Secondly, a cell wall element was placed at an angle determined from Equation (2-6) in the middle of two cell positions as shown in Fig. 2.14B. Finally, all cell wall elements were connected as shown in Fig. 2.14C[19].

The representative models with a slightly asymmetrical hexagonal shape under wet and oven-dried conditions of the early wood tracheid of *C. obtusa* are shown in Fig. 2.15. The solid and dotted lines represent wet and oven-dried conditions, respectively. The cell with an asymmetrical and hexagonal shape may rotate during drying, thus the shear deformation of cells should be taken into consideration when analyzing shrinkage. The included angles

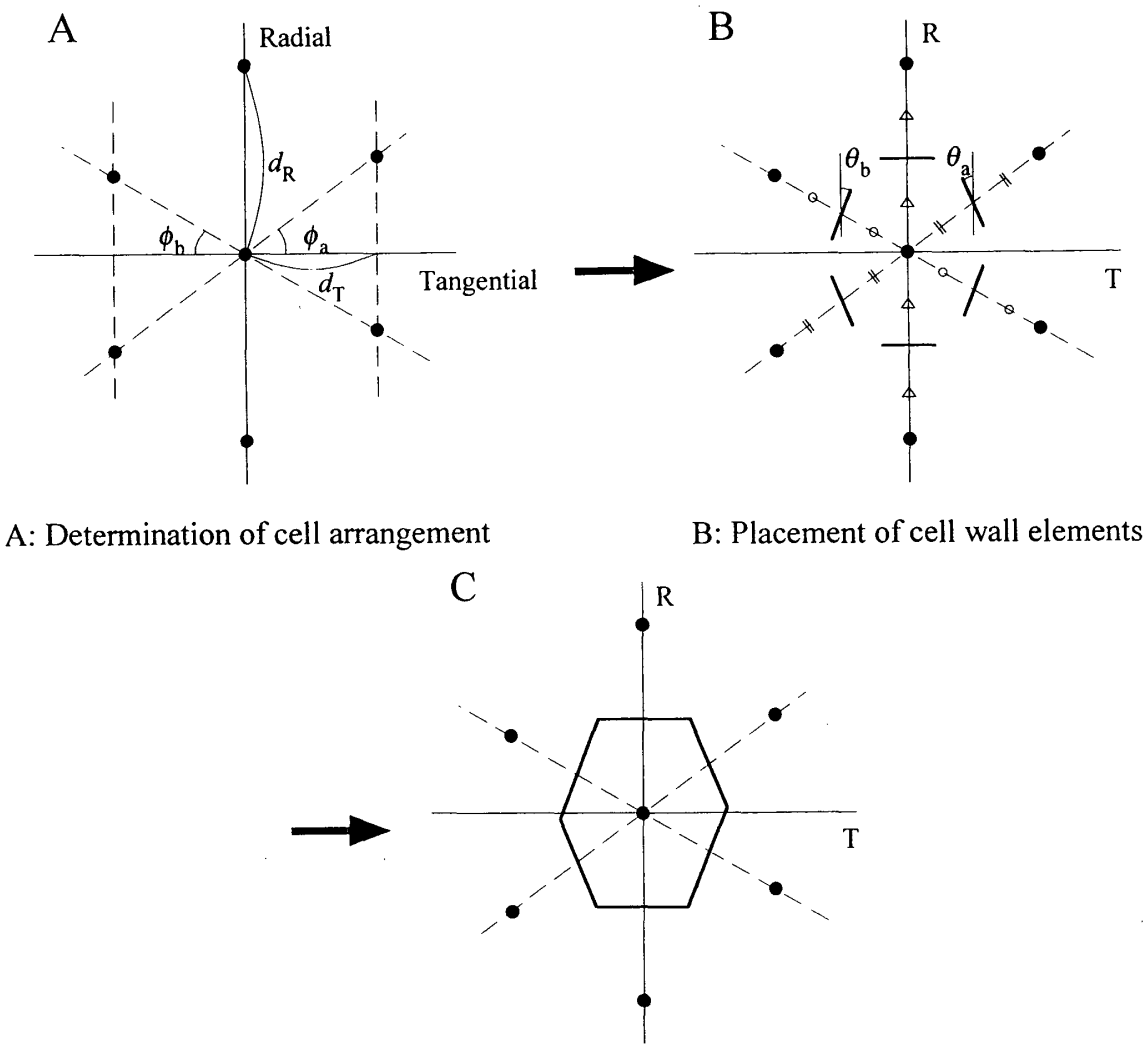

Fig. 2.14. A representative cell model constructed by the power spectrum analysis. d_R: the periodicity of cell positions in the radial direction determined by Equation (2-2), d_T: the periodicity of radial files in the tangentail direction determined by Equation (2-2), ϕ: the diection of cell arrangement determined by Equation (2-3), θ: the angle between the cell wall elements and the radial direction determined by Equation (2-6).

changed during drying. In these models, the included angles between two radial walls in wet (α) and oven-dried (β) conditions were 135° and 140°, respectively, so the angle increased by 5 degrees during drying. This result suggested that the tangential shrinkage of wood with hexagonal cell shapes resulted not only from the cell wall shrinkage but also from the change in cell shape. The shrinkages determined from the power spectrum agreed well with those measured by a caliper for block specimens. The axial shrinkages of elements A,

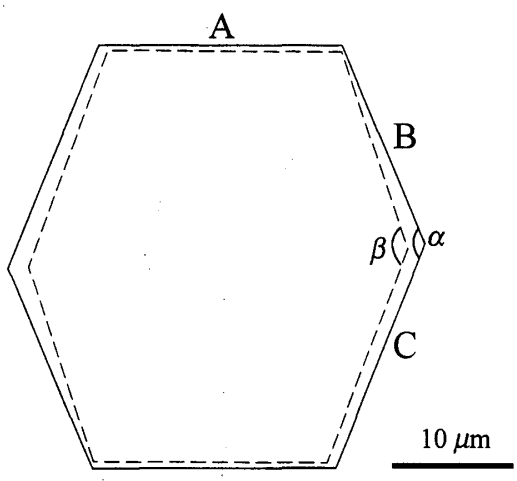

Fig. 2.15. A comparison of cell shapis in wet (solid line) and ovendried (dotted line) conditions for the early wood tracheid of *Chamaecyparis obtusa*. α: 135, β: 140.

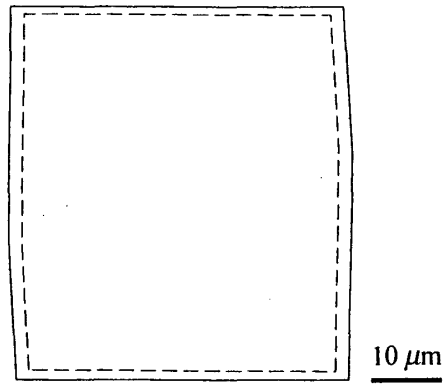

Fig. 2.16. A comparison of cell shapes in wet (solid line) and oven-dried (dotted line) conditions for the early wood trachied of *Picea sitchensis*.

Table 2.3. Shrinkages obtained by the power spectrum analysis for separated early woods of *Chamaecyparis obtusa* and *Picea sitchensis*. R: radial direction, T: tangential direction.

Species	Shrinkage (%)		T/R
	R	T	
Chamaecyparis obtusa	2.8	6.2	2.2
Picea sitchensis	4.6	7.8	1.7

B and C (Fig. 2.15) were 3.3%, 4.0% and 5.1%, respectively. On the other hand, the average axial shrinkages of the corresponding cell walls shown in Fig. 2.9B were 3.5%, 4.1% and 3.3%, respectively. Both the values were in agreement with each other, although for element C, the former was slightly larger. These results show that the power spectrum is effective for the analysis of cell deformation.

Fig. 2.16 shows the results for *P. sitchensis*. The model indicated a relatively square shape and the included angle was little changed by drying. Table 2.3 shows the shrinkages in the radial and tangential directions and the ratio of tangential shrinkage to radial shrinkage for *C. obtusa* and *P. sitchensis*. The T/R ratio was larger in *C. obtusa* than in *P. sitchensis*. The larger T/R ratio of *C. obtusa* resulted from a larger change in included angle. These results show that cell shapes largely associated with the anisotropic shrinkage in the transverse direction.

Chapter 3. Transverse Shrinkage Anisotropy of Coniferous Woods

3.1 Introduction

In the previous chapter, the shrinkage behavior of early wood tracheids in the transverse direction was investigated using the replica method and power spectrum analysis. It was suggested that the cell shapes of early wood were closely related to the anisotropic shrinkage of whole wood. In addition, the mechanical interactions between wood tissues such as early wood, late wood and ray tissue must be taken into account to clarify the shrinkage anisotropy in the transverse direction. Pentoney[14] and Nakato *et al.*[15] analyzed the transverse shrinkage anisotropy of coniferous wood using a two layered model composed of early wood and late wood. Boutelje discussed the transverse shrinkage anisotropy of coniferous wood with plexiglas cell models as well as two layered wood models[25]. They emphasized that the cell shape and cell arrangement of early wood related greatly to the transverse shrinkage anisotropy of coniferous wood.

In this chapter, the shrinkage behavior of three kinds of coniferous wood was discussed using representative cell models of early and late woods constructed by the replica method and power spectrum analysis, and the transverse shrinkage anisotropy was analyzed with a two layered model composed of the representative cell models.

3.2. Materials and Methods

3.2.1. Wood specimens

Three kinds of coniferous wood, *Picea glehnii* Mast., *Pinus densiflora* Sieb. et Zucc. and *Pinus radiata* D. Don were used. Average annual ring width and air-dried specific gravity for each species are shown in Table 3.1. Specimens for measurements of shrinkage and Young's modulus were prepared from the same block.

According to the procedure shown in Fig. 3.1, five early wood specimens (A), five late wood specimens (B) and ten specimens containing late wood and early wood (C) were prepared from the wood block. The sizes of specimens for each species are shown in the same figure. Lines along the radial and tangential directions were drawn on the transverse surface of C specimens to measure macroscopic shrinkages. All specimens were soaked in distilled water until saturated. The transverse surfaces of A and B specimens in wet condition were smoothed by a sliding microtome. The early wood portion in A specimens

Table 3.1. Average annual ring width and air-dried specific gravity for each species.

Species	Average annual ring width (mm)	Air-dried specific gravity
Pinus radiata	15.0	0.41
Pinus densiflora	2.6	0.54
Picea glehnii	3.2	0.37

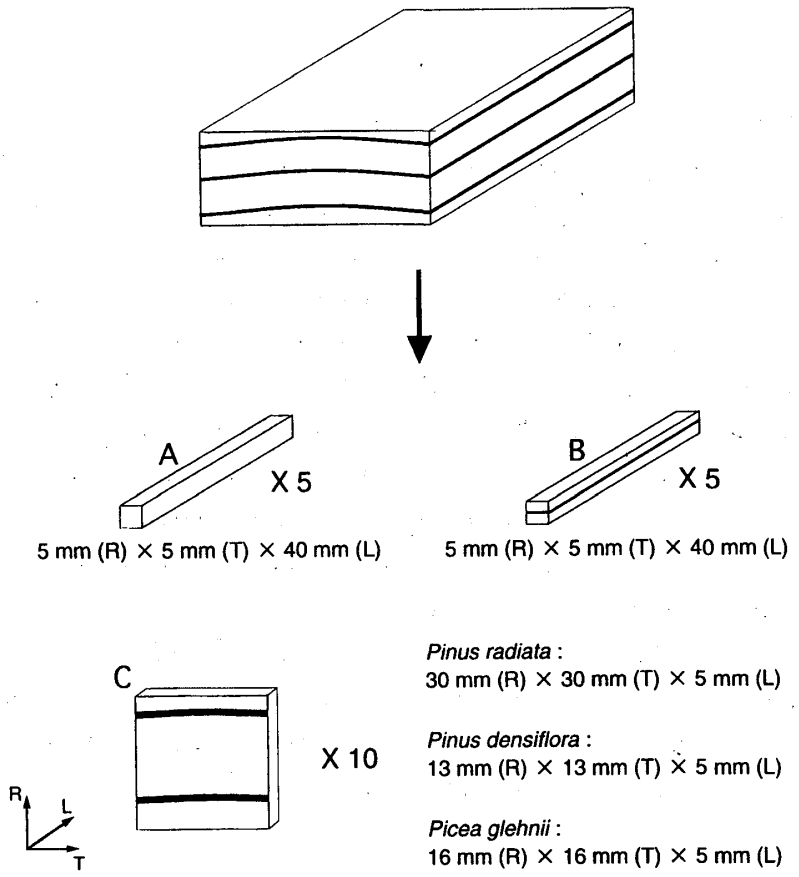

Fig. 3.1. The preparation of specimens for measurement of shrinkages. R: radial direction, T: tangential direction, L: longitudinal direction.

for *P. densiflora* and *P. glehnii* was separated from the late wood portion by a razor. The late wood portion in B specimens for three species was separated from the early wood portion using a razor. All A and B specimens were subjected to the replica method and power spectrum analysis to investigate the shrinkage behavior of tracheids on the transverse plane.

3.2.2. Construction of cell model and measurement of microscopic shrinkage

After all the surfaces of A specimens except the ones to be replicated were sealed with a thin polyvinylidene chloride film to avoid water evaporation, the specimens were pushed on a polyethylene film (0.1 mm thickness) softened by heating at about 130°C on a glass slide to obtain the replicas. The specimens were dried slowly at room temperature for five days, placed in a closed chamber conditioned at 98% R.H. for five days, dried over P_2O_5 at 60°C, and finally dried overnight at 105°C. After that, the replicas of the specimens under oven-dried condition were obtained.

Light micrographs were taken at three positions on the replicas prepared under wet and oven-dried conditions. Cell matrixes of 15 by 15 were set up on the micrographs. The edges between walls and lumens in the matrixes were traced onto a clear sheet. The traced figures were input into an image analyzing system (Luzex III) using a TV camera so that

Table 3.2. Sizes of D and E specimens.

Species	Specimen size (R: radial, T: tangential, L: longitudinal)
Pinus radiata	
D	15 mm (R)×100 mm (T)×1 mm (L)
E	10 mm (R)×100 mm (T)×1 mm (L)
Pinus densiflora	
D	2.6 mm (R)×40 mm (T)×1 mm (L)
E	1.0 mm (R)×40 mm (T)×1 mm (L)
Picea glehnii	
D	3.2 mm (R)×40 mm (T)×1 mm (L)
E	2.0 mm (R)×40 mm (T)×1 mm (L)

the radial direction of figures coincided with the axial direction of the monitor, smoothed and converted to binary figures. In the same procedure already explained in Chapter 2, the power spectra under wet and oven-dried conditions were obtained to construct the cell models of both conditions for each species. Furthermore, the microscopic shrinkages of specimens were calculated from the dimensional change of cell models constructed.

3.2.3. Measurement of macroscopic shrinkage and late wood fraction

C specimens were dried in the same manner mentioned above, and the radial and tangential shrinkages were calculated from the dimensional change of specimen measured by a traveling microscope. The radial width of the darker colored portion of C specimens was measured by a traveling microscope to determine the late wood fraction.

3.2.4. Measurement of tangential Young's modulus

For *P. glehnii* and *P. densiflora*, ten specimens containing one annual ring (D) as well as those containing only early wood (E) were prepared to measure the tangential Young's moduli. The sizes of specimens are shown in Table 3.2. After conditioned at 60% R.H. for about one week, the specimens were subjected to the measurement of tangential Young's modulus by the tensile forced oscillation method using an automatic dynamic viscoelastometer (ORIENTEC Co. Ltd., Rheovibron: DDV-25FP). The pre-load force applied to the specimens, span, measuring frequency, and temperature were 50 gf, 30 mm, 11 Hz and 20°C, respectively.

On the other hand, the preparation of wood specimens and the measurement of tangential Young's modulus for *P. radiata* with a wide annual ring were conducted according to the following procedure. Two wood blocks containing one annual ring (15 mm (R) by 50 mm (T) by 100 mm (L)) were glued at radial surfaces with polyvinyl acetate adhesive. Ten specimens (15 mm (R) by 100 mm (T) by 1 mm (L)) were prepared from the block to measure the tangential Young's modulus. Ten specimens (10 mm (R) by 100 mm (T) by 1 mm (L)) to measure the tangential Young's modulus of early wood were prepared in the same manner. After conditioned at 60% R.H. for about one week, the specimens were

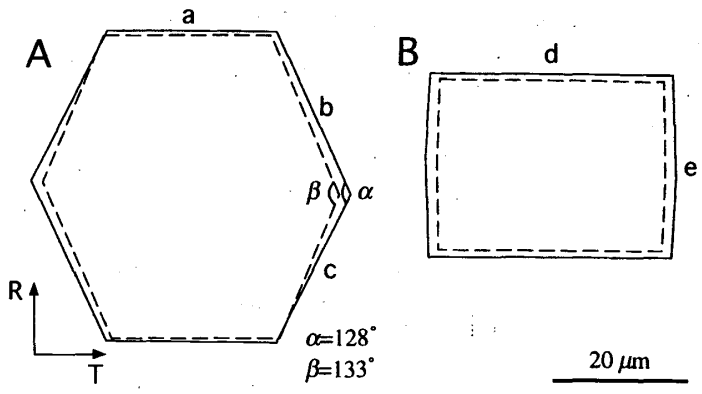

Fig. 3.2. Cell model shape in wet (solid line) and oven-dried (dotted line) conditions for early (A) and late (B) wood tracheids of *Pinus radiata*.

subjected to the measurement by a free-free flexural vibration method at 20°C. It has been confirmed that the glue line has no influence on the results[26].

3.3. Results and Discussion

3.3.1. Shrinkage behavior of early and late wood tracheids

Fig. 3.2 shows the representative cell model shapes of early (A) and late (B) wood tracheids for *P. radiata* constructed by the power spectrum analysis. The solid and dotted lines represent wet and oven-dried conditions, respectively. In Chapter 2, it was shown that the shrinkage determined by the power spectrum analysis for the center of gravity of each cell agreed well with the macroscopic shrinkage and the features of shrinkage deformation could be well expressed by the models constructed by the analysis. The representative model of early wood tracheids of *P. radiata* had a hexagonal and slightly asymmetrical shape. The cells rotated slightly during drying. The radial and tangential shrinkages of the model were 2.5% and 5.5%, respectively. The axial shrinkages of cell elements a, b and c were 4.2%, 3.7% and 6.2%, respectively. The included angles between two radial walls in wet (α) and oven-dried (β) conditions were 128° and 133°, respectively, so that the angle increased by 5 degrees during drying. The early wood tracheid itself showed anisotropic shrinkage with changing cell shape, which might cause the anisotropic shrinkage in the separated early wood. On the other hand, the transverse shape of late wood tracheids was almost rectangular. The radial and tangential shrinkages of the model were 7.2% and 8.0%, respectively. No rotation of cells was observed during drying. The included angle was slightly increased during drying. The axial shrinkages of cell elements d and e were 7.9% and 7.2%, respectively. Late wood tracheids showed almost isotropic shrinkage.

Fig. 3.3 shows the representative cell models of *P. densiflora*. Although the model shape of early wood tracheids was hexagonal, a distinct hexagonal cell shape such as that of *P. radiata* was not constructed. The relatively low symmetry in transverse cell shape was

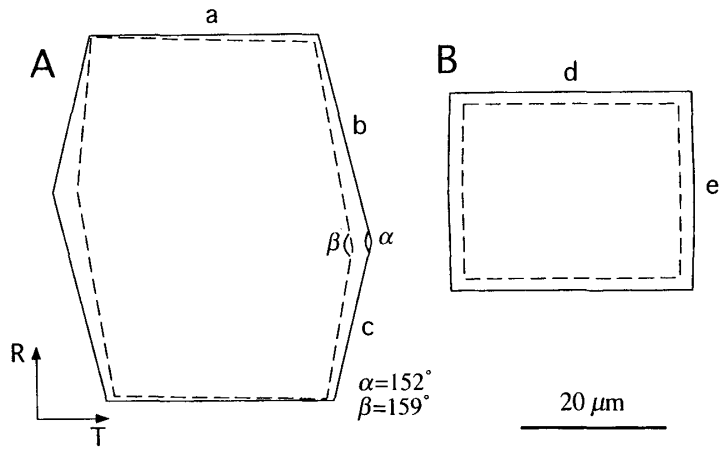

Fig. 3.3. Cell model shape in wet (solid line) and oven-dried (dotted line) conditions for early (A) and late (B) wood tracheids of *Pinus densiflora*.

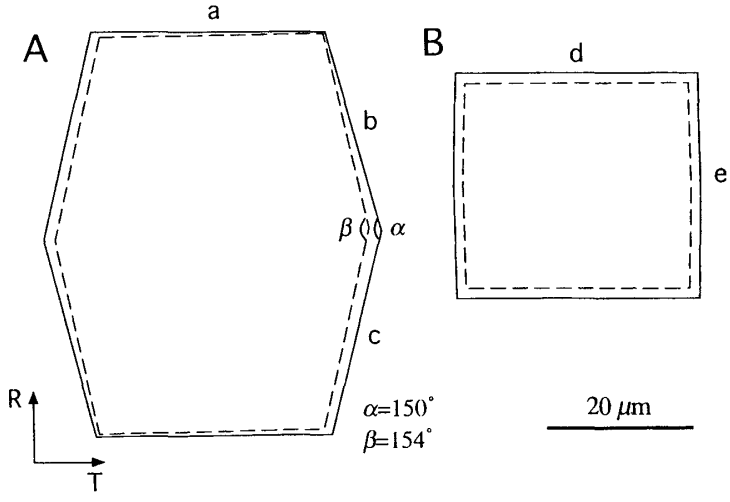

Fig. 3.4. Cell model shape in wet (solid line) and oven-dried (dotted line) conditions for early (A) and late (B) wood tracheids of *Picea glehnii*.

indicated from the models. The cells rotated slightly during drying. The radial and tangential shrinkages of the model were 2.0% and 5.6%, respectively. The axial shrinkages of cell elements a, b and c were 2.1%, 2.5% and 6.0%, respectively. The included angles between two radial walls in wet (α) and oven-dried (β) conditions were 152° and 159°, respectively, so that the angle increased by 7 degrees during drying. The early wood tracheid itself showed anisotropic shrinkage with changing cell shape. The late wood tracheid showed almost a rectangular shape. Almost isotropic shrinkage was observed. The radial and tangential shrinkages of the model were 11.4% and 11.0%, respectively. No rotation of cells and no change of included angle were observed during drying. The axial shrinkages of cell elements d and e were 11.9% and 11.2%, respectively.

Fig. 3.4 shows the representative cell models of *P. glehnii*. The model shape of early

wood tracheids was hexagonal and slightly asymmetrical. This model shape was significantly different from that of *P. sitchensis* shown in Fig. 2.16 in Chapter 2, although both species belonged to *Picea* genus. This result suggested that there was a difference in transverse cell shape among species even in the same genus. The cells rotated slightly during drying. The radial and tangential shrinkages of the model were 2.2% and 5.8%, respectively. The axial shrinkages of cell elements a, b and c were 5.3%, 2.9% and 2.4%, respectively. The included angles between two radial walls in wet (α) and oven-dried (β) conditions were 150° and 154°, respectively, so that the angle increased by 4 degrees during drying. The early wood tracheid of *P. glehnii* shrank more anisotropically than that of *P. sitchensis,* which ascribed to the difference in transverse cell shapes. The late wood tracheid showed almost a rectangular shape. Almost isotropic shrinkage was observed. The radial and tangential shrinkages of the model were 9.6% and 7.9%, respectively. No rotation of cells and no change of included angle were observed during drying. The axial shrinkages of cell elements d and e were 7.6% and 8.9%, respectively.

Different shrinkage behavior was observed between early and late wood tracheids, namely, early wood tracheids showed anisotropic shrinkage while late wood tracheids showed relatively isotropic shrinkage. In *P. densiflora* and *P. glehnii,* the shrinkage anisotropy of late wood tracheids was in contrast to that of early wood tracheids. The same result was reported for the late wood of *Pseudotsuga menziesii* Franco[14]. Therefore, to analyze the shrinkage anisotropy of coniferous wood with a low ray tissue volume fraction, the mechanical interaction between early wood and late wood must be taken into consideration.

3.3.2. Shrinkage anisotropy of coniferous wood

The microscopic shrinkages of early and late wood for three species were determined by the power spectrum analysis. Furthermore, the radial and tangential shrinkages of C specimens, the tangential Young's modulus of whole wood specimens and the tangential Young's modulus of early wood specimens were measured. These results are shown in Table 3.3. Using these values, the shrinkage of the two layered model were calculated to investigate the shrinkage anisotropy of coniferous wood.

Fig. 3.5 shows a model of coniferous wood in which layers *a* and *b* represent late and early wood, and directions 1 and 2 correspond to the tangential and radial directions, respectively[14,15]. The model A under wet condition may change to the model B after drying. A homogeneous strain may occur in the direction 1 but not in the edge portions in the direction 2, as shown in the model B. The shrinkages ε_i ($i=1, 2$) and stresses σ_i ($i=1, 2$) of the model can be expressed with the shrinkages ε_i^k and the stresses σ_i^k ($i=1, 2$; $k=a, b$) of early wood and late wood.

$$\begin{aligned} &\varepsilon_1=\varepsilon_1^a=\varepsilon_1^b,\ \sigma_1=\phi\sigma_1^a=\psi\sigma_1^b\ (=0),\\ &\varepsilon_2=\phi\varepsilon_2^a=\psi\varepsilon_2^b,\ \sigma_2=\sigma_2^a=\sigma_2^b\ (=0), \end{aligned} \tag{3-1}$$

Table 3.3. Experimental values of three species examined.

	Pinus radiata	*Pinus densiflora*	*Picea glehnii*
Tangential shrinkage ε_1 (%)	6.32	9.38	7.21
Radial shrinkage ε_2 (%)	2.54	4.86	2.27
Tangential shrinkage of late wood α_1^a (%)	8.01	11.01	7.86
Tangential shrinkage of early wood α_1^b (%)	5.46	5.55	5.82
Radial shrinkage of late wood α_2^a (%)	7.23	11.38	9.63
Radial shrinkage of early wood α_2^b (%)	2.52	2.01	2.22
Tangential Young's modulus E^1 (GPa)	0.42	0.72	0.45
Tangential Young's modulus of early wood E_1^b (GPa)	0.37	0.25	0.20

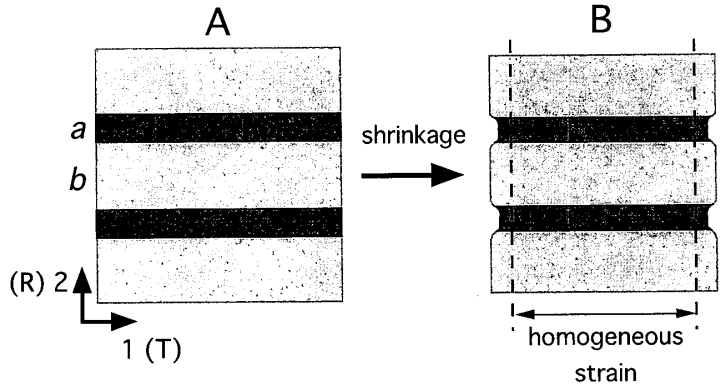

Fig. 3.5. Coniferous wood model. Layers *a* and *b* correspond to late and early wood, and directions 1 and 2 to tangenital and radial directions, respectively.

where ϕ and ψ $(=1-\phi)$ are late wood and early wood fractions, respectively. Assuming that elastic strains occur in *a* and *b* layers due to mechanical interaction during drying, the shrinkages of *a* and *b* layers can be expressed by the following equations.

$$\left.\begin{aligned}\varepsilon_1^a&=\frac{1}{E_1^a}\sigma_1^a-\frac{\nu_{21}^a}{E_2^a}\sigma_2^a+\alpha_1^a\\ \varepsilon_1^b&=-\frac{\nu_{12}^b}{E_1^b}\sigma_1^b+\frac{1}{E_2^b}\sigma_2^b+\alpha_1^b\end{aligned}\right\} \tag{3-2a}$$

$$\left.\begin{aligned}\varepsilon_2^a&=\frac{1}{E_1^a}\sigma_1^a-\frac{\nu_{21}^a}{E_2^a}\sigma_2^a+\alpha_2^a\\ \varepsilon_2^b&=-\frac{\nu_{12}^b}{E_1^b}\sigma_1^b+\frac{1}{E_2^b}\sigma_2^b+\alpha_2^b\end{aligned}\right\} \tag{3-2b}$$

where E_i^k $(i=1, 2; k=a, b)$ are the elements of the matrix and α_i^k $(i=1, 2; k=a, b)$ are the shrinkages of layers. From these equations, ε_1 and ε_2 are given by

$$\varepsilon_1=\lambda\alpha_1^a+(1-\lambda)\,\alpha_1^b \tag{3-3a}$$

$$\varepsilon_2=\phi\alpha_2^a+\psi\alpha_2^b+C \tag{3-3b}$$

$$E_1=\phi E_1^a+\psi E_1^b, \tag{3-3c}$$

where λ and C are $\phi E_1^a/E_1$ and $(\alpha_1^b-\alpha_1^a)\{\psi\nu_{12}^b\lambda-\phi\nu_{12}^a(1-\lambda)\}$, respectively. The Poisson's ratios of late and early wood portions, ν_{12}^a and ν_{12}^b (the ratio of the strain in the direction 1 to that in the direction 2), are required to calculate the shrinkage in the direction 2. Generally, the Poisson's ratio of cellular solids can be determined by the geometrical calculation of the cell shape. Regarding the asymmetrical shapes of early wood tracheids shown in Fig. 3.2A, 3.3A and 3.4A as symmetrical ones, ν_{12}^b of three species were determined by the following expression[27],

$$\nu_{12}^b=\frac{(a/b+\sin\theta)\sin\theta}{\cos^2\theta}, \tag{3-4}$$

where a/b is the ratio of the axial length of cell element a to that of cell element b. The value of ν_{12}^b was calculated to be 0.74 for *P. radiata*, 0.38 for *P. densiflora* and *P. glehnii*. However, this equation cannot provide the Poisson's ratio of the late wood portion in which tracheids have lower θ values. For convenience, ν_{12}^a was assumed to be 0.5.

Substituting the experimental values of *P. radiata* shown in Table 3.3 for Equation (3-3a), a value of 0.25 was obtained for ϕ. Then, a value of 0.57 GPa was estimated for E_1^a. On the other hand, a value of 0.06 was obtained by substituting the values for Equation (3-3b). In this case, a value of 1.20 GPa was estimated for E_1^a. The experimental value of ϕ for C specimens was 0.17. In this case, a value of 0.66 GPa was obtained for E_1^a.

Substituting the experimental values of *P. densiflora* shown in Table 3.3 for Equation (3-3a), a value of 0.15 was obtained for ϕ. Then, a value of 3.35 GPa was estimated for E_1^a. A value of 0.37 was obtained by substituting the values for Equation (3-3b). In this case, a value of 1.51 GPa was estimated for E_1^a. Using 0.35 for the experimental value of ϕ, a value of 1.57 GPa was obtained for E_1^a.

Substituting the experimental values of *P. glehnii* shown in Table 3.3 for Equation (3-3a), a value of 0.30 was obtained for ϕ. Then, a value of 1.01 GPa was estimated for E_1^a. A value of 0.07 was obtained by substituting the values for Equation (3-3b). In this case, a value of 3.65 GPa was estimated for E_1^a. Using 0.20 for the experimental value of ϕ, a value of 1.41 GPa was obtained for E_1^a.

There was a difference between ϕ calculated from Equations (3-3a) and (3-3b) for three species examined. This difference was considered to originate in the simple analysis using a two layered model. However, the experimental values of ϕ were within the range between two calculated values. Therefore, it was considered that the analysis of transverse shrinkage behavior by the two layered model was valid as a first approximation.

The shrinkage anisotropy of coniferous wood was predicted from Equations (3-3a) and (3-3b) with the experimental values of ϕ and E_1^a calculated using the experimental ϕ, namely, $\phi=0.17$ and $E_1^a=0.66$ GPa for *P. radiata*, $\phi=0.35$ and $E_1^a=1.57$ GPa for *P. densiflora*,

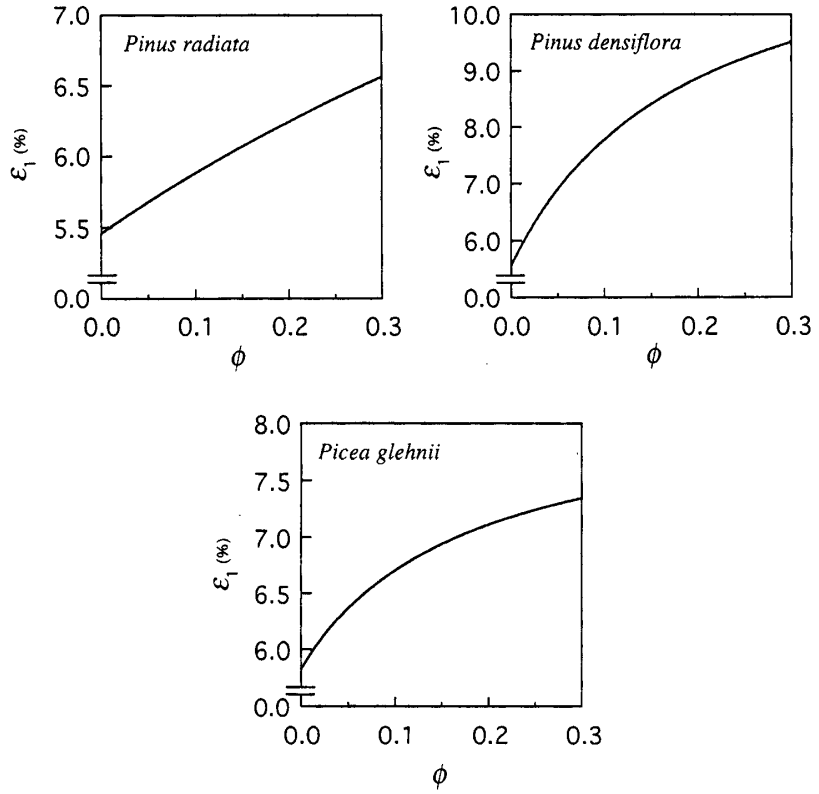

Fig. 3.6. Relathionship between calculated values of tangential shrinkage ε_1 and late wood fraction ϕ for three species.

and $\phi=0.20$ and $E_1^a=1.41$ GPa for *P. glehnii*.

Fig. 3.6 shows the relationship between the tangential shrinkage ε_1 and the late wood fraction ϕ for three species. The solid line represents the calculated values, which increased with increasing ϕ. Fig. 3.7 shows the relationship between the radial shrinkage ε_2 and ϕ. The solid line shows the values calculated by Equation (3-3b), and the dotted line shows the values calculated without the interaction term C. Although both values increased with increasing ϕ, the dotted line increased more rapidly. Fig. 3.8 shows the relationship between the shrinkage anisotropy $\varepsilon_1/\varepsilon_2$ and ϕ. The dotted line decreased more rapidly with increasing ϕ. The solid line of *P. densiflora* increased in the range of ϕ from 0 to 0.08, then decreased with increasing ϕ. These results show that the influence of the mechanical interaction on $\varepsilon_1/\varepsilon_2$ is significant.

Since $\psi\nu_{12}^b\lambda$ was about three times to five times larger than $\phi\nu_{12}^a(1-\lambda)$, the effect of $\psi\nu_{12}^b\lambda$ on C is remarkable.

$$\psi\nu_{12}^b\lambda=\psi\nu_{12}^b\frac{\phi E_1^a}{\phi E_1^a+\psi E_1^b}. \tag{3-5}$$

This equation contains the early wood fraction ψ, and the Poisson's ratio of early wood ν_{12}^b, the Young's modulus of late wood E_1^a and the Young's modulus of early wood E_1^b. If E_1^a

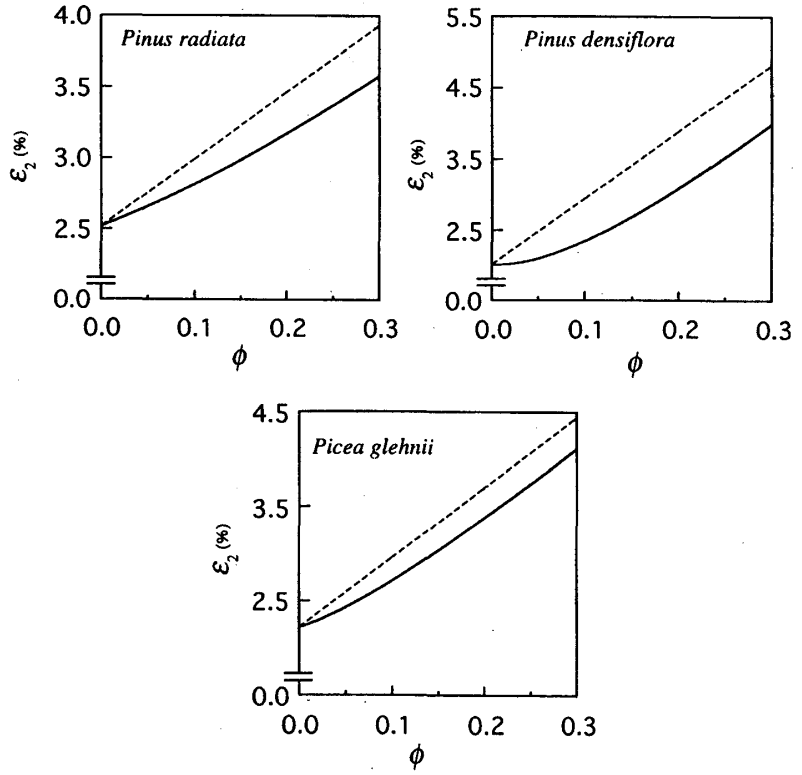

Fig. 3.7. Relationship between calculated values of radial shrinkage ε_2 and late wood fraction ϕ. Solid and dotted lines show the results from Equation (3-3b) and the equation without the interaction term C, respectively.

can be measured, it can be estimated as a constant value because there is almost no difference in the transverse shapes of late wood tracheids among species. Therefore, C is considered to depend more significantly on both ν_{12}^b and E_1^b. These results suggest that the shrinkage anisotropy of coniferous wood depends remarkably on the transverse shape of early wood tracheid.

Chapter 4. Tangential Young's Modulus of Coniferous Early Woods

4.1 Introduction

As in the case of the transverse shrinkage, the transverse Young's modulus is different among wood species when compared at the same specific gravity. This may result mainly from both the transverse shapes of early wood tracheids and the late wood fraction, since the shapes of late wood tracheids are considered to be almost the same regardless of species. However, there are few reports which investigated the effects of cellular structures on the transverse Young's modulus.

The power spectrum analysis is effective for the theoretical analysis of the transverse Young's modulus, because the cell models for the specimens subjected to the measurements

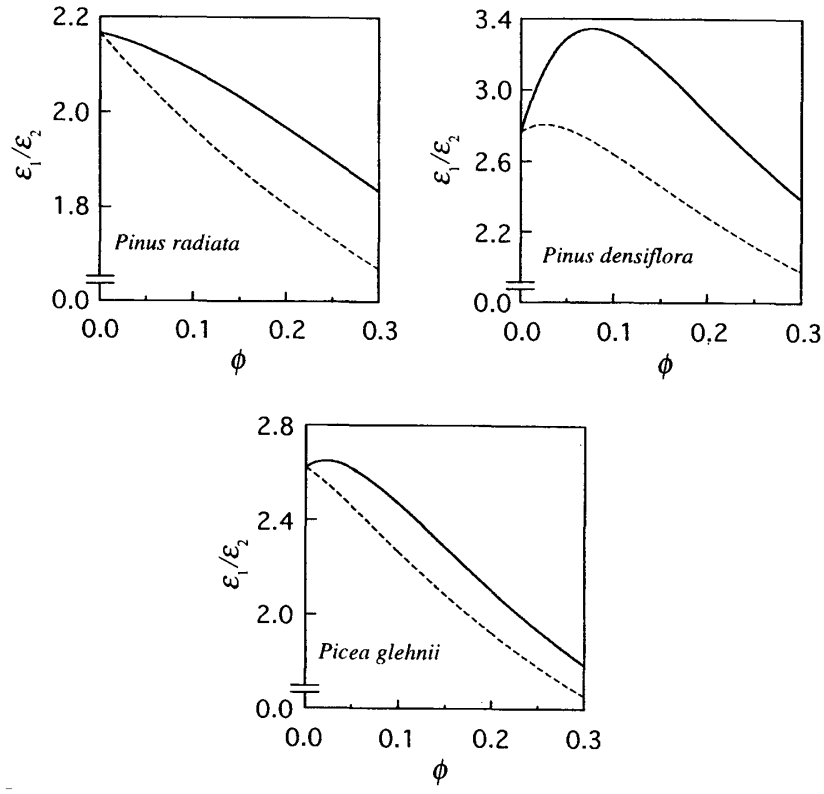

Fig. 3.8. Relationship between shrinkage anisotorpy $\varepsilon_1/\varepsilon_2$ and late wood fraction ϕ. Solid and dotted lines show the results with and without the interaction term C, respectively.

can be constructed by it. In this chapter, the dynamic Young's moduli of early woods in the tangential direction for seven kinds of coniferous wood were measured and representative cell models of the specimens subjected to the measurements were constructed by the power spectrum analysis. The effects of the transverse cell shapes on the tangential Young's modulus were examined comparing the calculated values with the experimental ones.

4.2. Materials and Methods

4.2.1. Wood specimens

The early wood of seven kinds of conifer, *Chamaecyparis obtusa* Endl., *Cryptomeria japonica* D. Don, *Metasequoia glyptostroboides* Hu et Cheng, *Picea glehnii* Mast., *Pinus densiflora* Sieb. et Zucc., *Pinus radiata* D. Don, and *Tsuga heterophylla* Sarg. were used.

4.2.2. Measurements of dynamic Young's modulus and specific gravity

Twenty specimens of 1 mm (longitudinal) by 2 mm (radial) by 40 mm (tangential) were prepared from each species. After conditioned at 60% R.H. for about 10 days, the specimens were subjected to the measurement of tangential Young's modulus E_T using Rheovibron DDV-25FP (ORIENTEC Co. Ltd.). The pre-load force applied to the specimens, span, measuring frequency, and temperature were 50 gf, 30 mm, 11 Hz and

20°C, respectively.

Immediately after the measurements, the weights and dimensions of specimens were measured using an electric balance and a traveling microscope to obtain the densities of specimens γ.

4.2.3. Cell model Construction

After the measurements of the Young's modulus E_T and the specific gravity γ, three specimens for each species with medium values were selected to construct a cell model.

Small pieces cut from the specimens were soaked in distilled water, then dehydrated through a graded series of ethanol and propylene oxide, before being embedded in Spurr's resin. Transverse sections with 2 μm thickness were cut from the embedded pieces using an ultramicrotome (Ivan Sovall MT-1) and then mounted in Canada balsam after staining with safranine. These sections were photographed under a light microscope.

The micrographs were input into a computer through an image scanner. Images with a size of 1,024 by 1,024 pixels on which 20 by 20 cell matrixes were set up were made from the input images, smoothed, and transformed to binary images with gray levels of 255 and 0. UTHSCSA Image Tool (version 1.25.) and Paint Shop Pro (version 3.0.) were used for these treatments. About 4,000 cells for each species were subjected to the following power spectrum analysis.

The center of gravity for each cell was derived from the binary images and shown by a dot containing a single Gaussian-profile peak with a sectional rms width of three pixels. The power spectrum of this image was obtained by the fast Fourier transform to determine the periodicity and direction of cell arrangement. Semper for Windows 6.4.6 (Synoptics Ltd.) was used for these analyses. The cell wall regions in the binary images were skeletonized using Scion Image PC and the spectrum was obtained using Semper for Windows 6.4.6 to estimate the two dimensional orientation of the cell walls. As a first approximation, the power spectra of all species were regarded to be almost symmetrical, and a representative cell model with a symmetrical shape for each species was constructed in the same manner described in Chapter 2.

The axial lengths of the tangential and radial cell walls, T and R, the double cell wall thickness t, and the element angle θ of the cell model shown in Fig. 4.1 were determined for each species. The cell wall thickness t can be determined using the following equation which gives the specific gravity of the cell model γ,

$$\frac{\gamma}{\gamma_w} = \frac{(t/R)\,(T/R+2)}{2\cos\theta\,(T/R+\sin\theta)}, \tag{4-1}$$

where γ_w is the specific gravity of the cell wall[27]. It is reported that γ_w of wood at 20°C and 60% R.H. is 1.43 g/cm^3 [28]. The area S and the aspect ratio λ (the ratio of radial diameter to tangential diameter) of the cell model were determined.

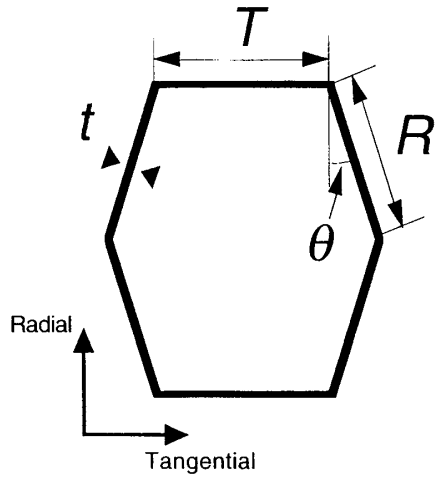

Fig. 4.1. Geometric parameters of a cell model.

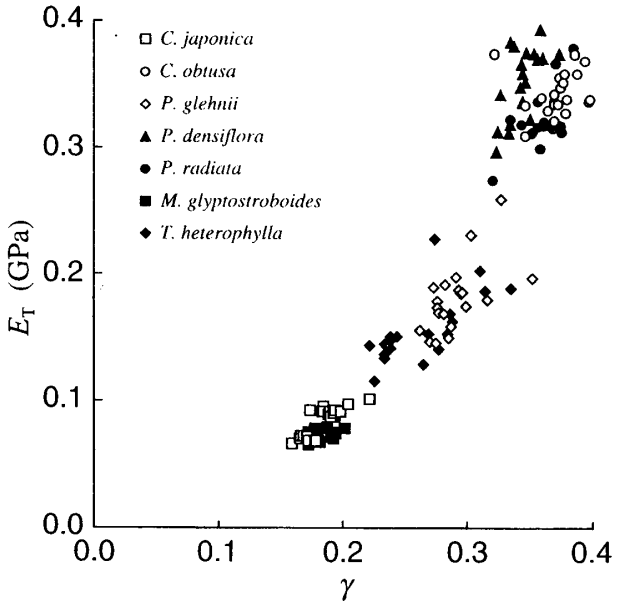

Fig. 4.2. Relationship between tangential Young's modulus E_T and specific gravity γ for all specimens.

Table 4.1. Elastic constants of a microfibril and matrix substance.

Elastic constant	E_x	$E_y=E_z$	G_{yz}	$G_{zx}=G_{xy}$	ν_{yz}	ν_{zx}	ν_{xy}
Microfibril	134	27.2	13.0	4.40	0.04	0.02	0.10
Matrix substance	2.00	2.00	0.77	0.77	0.30	0.30	0.30

E (GPa): directional Young's modulus, G (GPa): shear modulus, ν: Poisson's ratio, x: direction parallel to microfibril length, y and z: direction perpendicular to x.

4.2.4. Calculation of the tangential Young's modulus of a cell model

Gibson and Ashby discussed the in-plane properties of honeycombs and proposed constitutive equations when a honeycomb was loaded biaxially[27]. Their equations were adopted to calculate the tangential Young's modulus of the cell model E_T. By substituting zero for the stress in the radial direction, the following equation can be obtained,

$$\frac{1}{E_T}=\frac{\cos\theta\,(2T/R+\sin^2\theta)}{(t/R)\,(T/R+\sin\theta)\,E_a}+\frac{\cos^3\theta}{(t/R)^3\,(T/R+\sin\theta)\,E_b}, \tag{4-2}$$

where E_a and E_b are the axial and bending Young's moduli of the cell wall in the perimetric direction. The first and second terms represent the axial and bending contributions to E_T, respectively. E_a was determined using a double cell wall model with complete shear restraint[29] after Chou *et al.*[30], Tang *et al.*[31] and Ohgama *et al.*[32]. E_b was calculated on the basis of the symmetric laminate theory[33] using the same double cell wall model. The elastic constants of a microfibril and matrix substance are shown in Table 4.1, and the volume fractions and the microfibril angles of the cell wall layers are shown in Table 4.2.

Table 4.2. Volume fractions and microfibril angles of cell wall layers.

Cell wall layer	I+P	S_1	S_1	S_2	S_3
Volume fraction of cell wall layers	0.07	0.04	0.04	0.80	0.05
Volume fraction					
Microfibril	0.10	0.53	0.53	0.53	0.53
Matrix substance	0.90	0.47	0.47	0.47	0.47
Microfibril angle (°)	90	67	−67	6	82

I: intercellular layer, P: primary wall, S: secondary wall

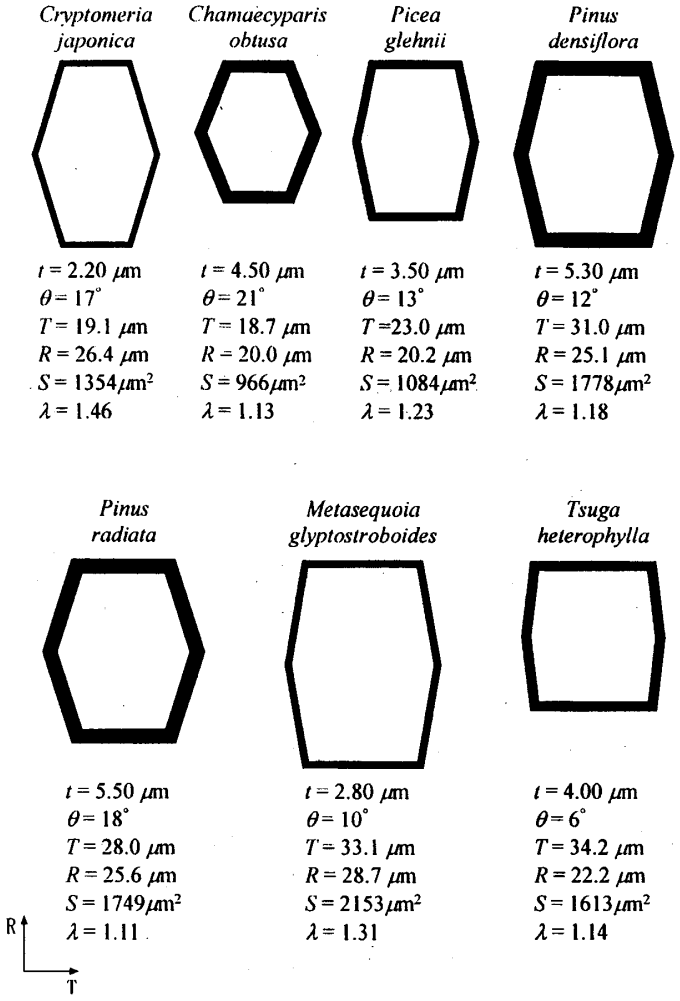

Fig. 4.3. Cell models and geometric parameters for seven species.

4.3. Results and Discussion

4.3.1. Relationship between tangential Young's modulus and cell shape

Fig. 4.2 shows the relationship between E_T and γ at 11 Hz for all specimens measured. E_T increased curvilinearly with increasing γ. Above γ=0.30, E_T remarkably increased. It differed significantly among species when compared at the same γ. These results

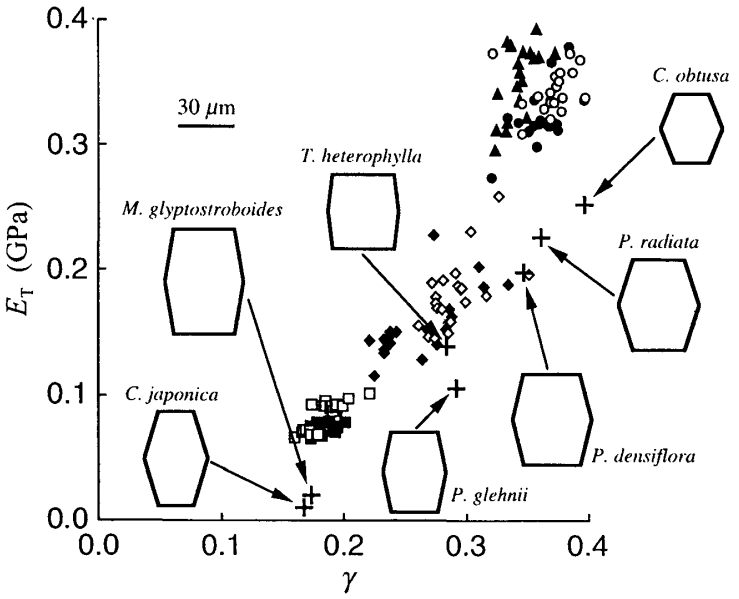

Fig. 4.4. Comparison between experimental and calculated (cross symbols) tangential Young's moduli. Refer to Fig. 4.2 for the legends of experimental values.

suggested that E_T was affected by both γ and the transverse cell shape.

Fig. 4.3 shows the cell models constructed by the power spectrum analysis for seven species. The cell wall thickness t, the element angle θ, the axial lengths of tangential and radial cell walls, T and R, the area S, and the aspect ratio λ are also shown in the same figure. The shapes of all species were hexagonal. θ of *T. heterophylla* was very small, so the model showed nearly a square shape. On the other hand, θs of *C. obtusa* and *P. radiata* were relatively large, so the models had distinct hexagonal shapes. The model shape of *C. japonica* with the largest λ of 1.46 was long in the radial direction. *P. radiata* had the smallest λ of 1.11. *C. obtusa* had the smallest S, while *M. glyptostroboides* had the largest S.

4.3.2. Tangential Young's moduli of cell models

To calculate E_T of the cell model using Equation (4-2), the geometric parameters of the cell model shown in Fig. 4.3 were used. E_a and E_b were calculated to be 14.3 GPa and 15.6 GPa and these values were used to calculate E_T. The calculated results of E_T are compared with the experimental ones in Fig. 4.4. Cross symbols in the figure indicate the calculated values. The cell models of seven species are also shown in the figure. The calculated values were smaller than the experimental values when compared at the same γ. Uniform wall thickness along the axial length of cell wall was assumed to calculate E_T. However, in reality it is not uniform, being somewhat thicker around cell corners, as shown in Fig. 4.5. Since this results in a reduction in the bending deformation of the cell wall, the small calculated values may be ascribed to it. Although a quantitative agreement between the calculated and experimental results was not obtained, the calculated results explained

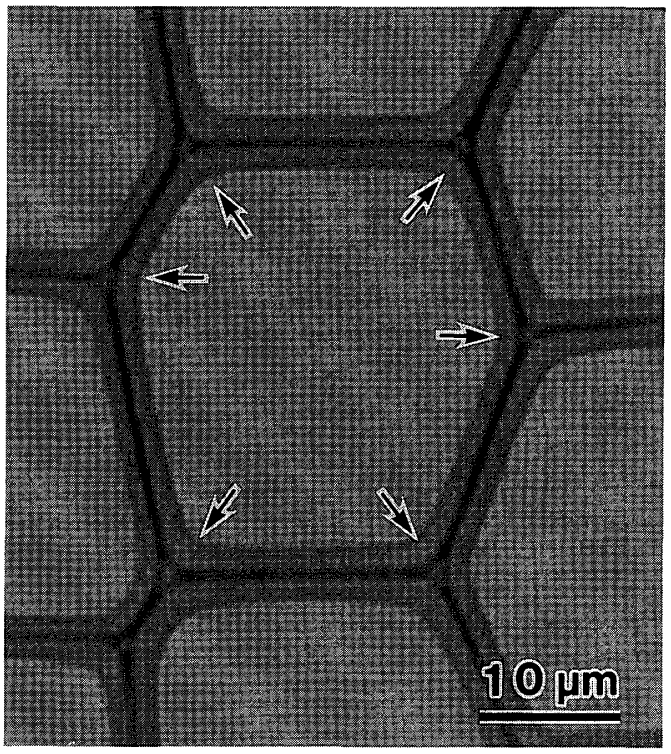

Fig. 4.5. Transverse cell shape of *Picea glehnii*. Cell walls around the corner (arrows) are thick.

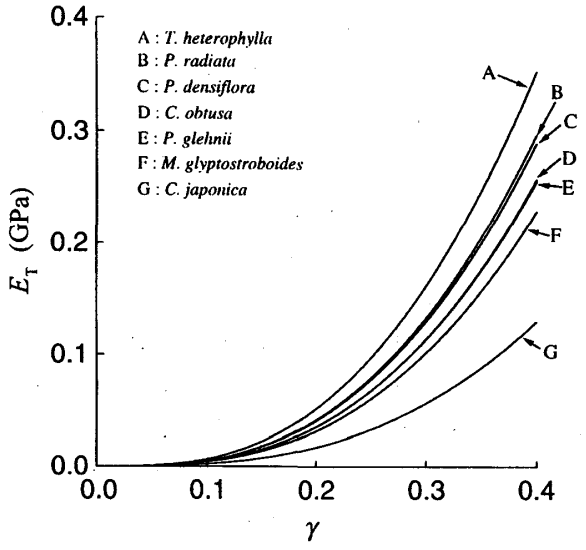

Fig. 4.6. Relationship between tangential Young's modulus E_T and specific gravity γ when cell wall thickness t changed.

qualitatively the change of E_T with γ as well as the difference in E_T among species.

4.3.3. Effect of geometric parameter on Young's modulus and specific gravity

E_T and γ of the cell model vary with geometric parameters. Fig. 4.6 shows the

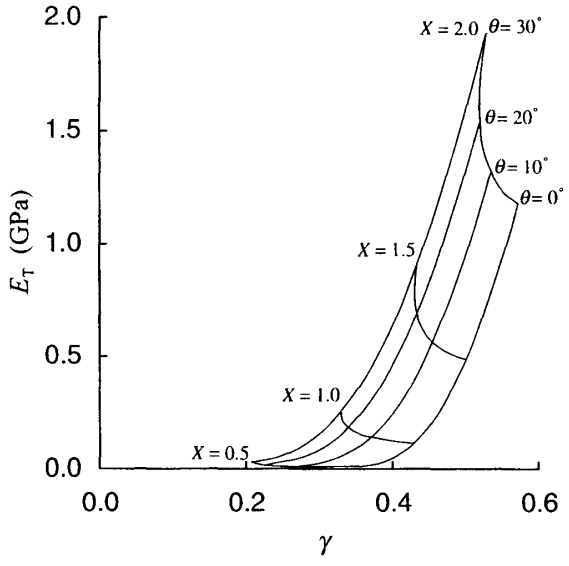

Fig. 4.7. Relationship between tangential Young's modulus E_T and specific gravity γ at indicated element angles θs and ratios of the axial length of tangential wall to that of radial wall Xs when tangential wall length T and cell wall thickness t were fixed at 20 μm and 4 μm, respectively.

relationship between E_T and γ when t changed. Although E_T increased with increasing γ in all models, values greatly differed at the same γ. E_T was the largest in the model of *T. heterophylla* and the smallest in that of *C. japonica*. For example, the ratio of the former to the latter was about 4 at γ=0.40.

Fig. 4.7 shows the relationship between E_T and γ at indicated θs and Xs (=T/R), where T and t were fixed at 20 μm and 4 μm, respectively. E_T rapidly increased with γ when X increased at respective θs and increased with decreasing γ when θ increased at respective Xs. The increase in E_T with θ became remarkable with increasing X. Fig. 4.8 represents the relationship of E_T with γ at indicated θs and Xs, where R and t were fixed at 20 μm and 4 μm, respectively. E_T decreased with increasing γ when X increased at respective θs and increased with increasing θ at respective Xs. In particular, it greatly increased without a remarkable change in θ at larger Xs. At X=1.5, E_T increased up to about 2.0 times by change of θ from 0° to 30° while the decrease in γ was about 13%. These results suggested that θ was a significant factor affecting E_T among cells with the same X.

Fig. 4.9 shows the ratio of the bending contribution to the axial one B/A where A and B represent the first and second terms in Equation (4-2), respectively. B/A increased with decreasing θ at respective Xs. When compared at the same θ, B/A increased with decreasing X. The bending contribution increased and E_T decreased with a decrease of both X and θ nevertheless γ increased.

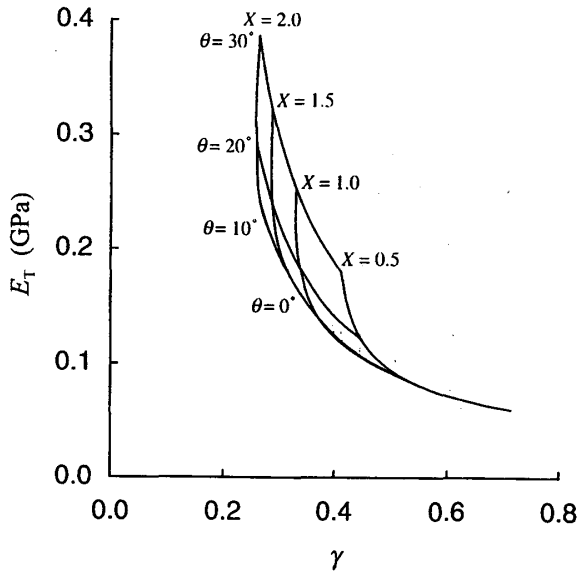

Fig. 4.8. Relationship between trangential Young's modulus E_T and specific gravity γ at indicated element angles θs and ratios of the axial length of tangential wall to that of radial wall Xs when radial wall length R and cell wall thickness t were fixed at 20 μm and 4 μm, respectively.

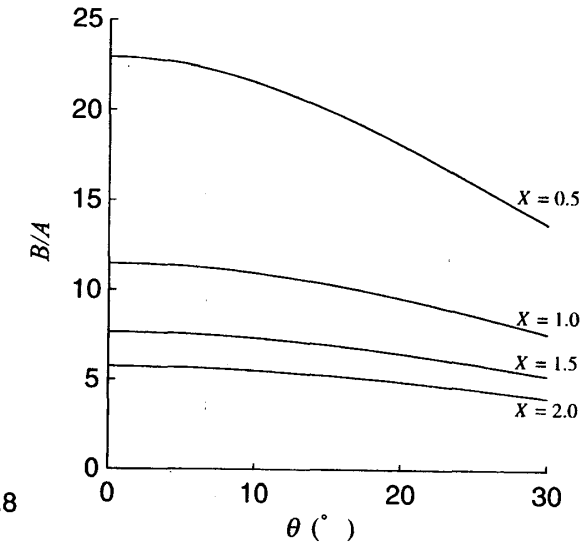

Fig. 4.9. Relationship between the ratio of bending contribution to axial one B/A and element angle θ.

Conclusion

In Chapter 1, the relationships among the specific gravities, the shrinkages and the Young's moduli were investigated in normal and compression woods of *Cryptomearia japonica*, *Chamaecyparis obtusa* and *Picea sitchensis* as well as in *Agathis bornensis* and *Podocarpus imbricatus* which are tropical conifers. The darkly colored wood portions of *A. bornensis*, which are randomly distributed all over the transverse surface of a stem, showed the typical features of compression wood. Anisotropic shrinkage was observed in the transverse directions of *A. bornensis* and *P. imbricatus*, which have no distinct growth rings. In the longitudinal direction, there was no definite correlation between the shrinkage and the specific gravity for normal wood, whereas the shrinkage for compression wood increased with increasing specific gravity. In the radial direction, the shrinkage of normal wood generally increased with increasing specific gravity, whereas no clear correlation was observed for compression wood. In the tangential direction, there was no correlation for either normal or compression wood. In the radial and tangential directions, no clear correlation was observed between the shrinkage and the Young's modulus for either normal wood or compression wood except for normal wood in the radial direction. On the other hand, there was a high correlation between the shrinkage and the specific Young's modulus in the

longitudinal direction for both normal and compression woods. This relationship was expressed by a hyperbolic equation.

In Chapter 2, the replica method and power spectrum analysis were used to investigate the shrinkage behavior of the normal wood tracheids of *Cryptomearia japonica, Chamaecyparis obtusa, Picea sitchensis* and *Agathis bornensis,* and the compression wood tracheids of *C. japonica* and *C. obtusa.* Cell lumens shrank in normal wood and expanded in compression wood during drying. The difference in this behavior was considered to depend on cell wall structures. The cell wall shrinkage in compression wood tracheid was generally larger than that in normal wood tracheid. This indicated that a higher extent of lignification was not always related to a low shrinkage in compression wood. The tracheids of *A. bornensis* with no distinct growth rings also shrank anisotropically in the transverse direction. The shrinkage behavior of tracheids for *C. obtusa* and *P. sitchensis* was shown by the cell models before and after shrinkage constructed by the power spectrum analysis. It was considered that the difference in shrinkage anisotropy among species greatly depended on their transverse cell shape.

In Chapter 3, the transverse shrinkage behavior of early wood and late wood tracheids of *Pinus radiata, Pinus densiflora* and *Picea glehnii* was investigated by the power spectrum analysis. The representative cell model shapes before and after shrinkage constructed by the analysis revealed that the early wood tracheid itself showed anisotropic shrinkage although the late wood tracheid showed almost isotropic shrinkage. To link up the macroscopic shrinkage of coniferous wood with the results obtained by the power spectrum analysis, a two layered model composed of early wood and late wood was adopted and the relationship between shrinkage anisotropy and late wood fraction was predicted. The results suggested that the shrinkage anisotropy depended significantly on the mechanical interaction between early and late wood.

In Chapter 4, the tangential Young's moduli of coniferous early woods for *Chamaecyparis obtusa, Cryptomearia japonica, Metasequoia glyptostroboides, Picea glehnii, Pinus densiflora, Pinus radiata* and *Tsuga heterophylla* were measured and representative cell models for the specimens subjected to the measurements were constructed by the power spectrum analysis. The experimental Young's modulus increased curvilinearly with increasing density, but differed significantly among species when compared at the same density. The bending Young's modulus of the wood cell wall in the perimetric direction was calculated on the basis of the symmetric laminate theory. A value of 15.6 GPa was obtained. Although the representative cell models of all species constructed by the power spectrum analysis were hexagonal in shape, that of *T. heterophylla* was nearly square, while those of *C. obtusa* and *P. radiata* were distinctly hexagonal. The calculated Young's moduli of the cell models qualitatively agreed with the experimental values. The calculated Young's modulus at the same density greatly differed depending on the cell models. It greatly increased with

increasing element angle without a remarkable change in the density at the larger ratios of the axial length of tangential wall to that of radial wall.

Acknowledgment

The author wishes to express his sincere thanks to Professor Dr. Misato Norimoto, Wood Research Institute, Kyoto University, for his proper direction and kind encouragement during the entire course of this study.

The author is deeply grateful to Professor Dr. Minoru Fujita, Graduate School of Agriculture, Kyoto University, for his kind guidance in power spectrum analysis, and also for his valuable suggestions and critical readings of this manuscript. The author is deeply grateful to Professor Dr. Shuichi Kawai, Wood Research Institute, Kyoto University, for his critical readings and valuable suggestions of this manuscript.

The author wishes to express his special thanks to Associate Professor Dr. Toshiro Morooka, Wood Research Institute, Kyoto University, for his help and discussions in the analysis of the Young's modulus of cell models. The author wishes to express his special thanks to Dr. Joseph Gril, Laboratoire de Mecanique et Genie Civil, Universite Montpellier 2, for his help and discussions in the analysis of transverse shrinkage using a two layered model. The author wishes to express his special thanks to Professor Dr. Toshimasa Ohgama, Faculty of Education, Chiba University, for his suggestions on the calculation of the Young's modulus of the cell wall. The author wishes to express his special thanks to Professor Dr. Yuji Imamura, Wood Research Institute, Kyoto University, for his discussion on the anatomical structures of tropical coniferous woods.

The author greatly appreciates to Mr. Kuniharu Yokoo, Fuyo Lumber Sales Co., Ltd., Professor Dr. Yoshinori Kobayashi, Institute of Wood Technology, Akita Prefectural College of Agriculture, Mr. Takayuki Sasaki, Kawai Musical Instruments Mfg. Co., Ltd. and Associate Professor Dr. Kunio Tsunoda, Wood Research Institute, Kyoto University, for their offering wood specimens. The author also greatly appreciates to Professor Dr. Jun Ohtani and Instructor Dr. Yuzou Sano, Graduate School of Agriculture, Hokkaido University, for their offering wood specimens.

The author wishes to express his thanks to Mr. Akio Adachi, Technical Officer of Wood Research Institute, Kyoto University, for his great support in the preparation of wood specimens. The author also wishes to express his thanks to Dr. Eiichi Obataya, Wood Research Institute, Kyoto University, for his proper advice on the experiment in this study. The author also wishes to express his thanks to Laboratory of Cell Structure and Function, Wood Research Institute, Kyoto University, especially to Dr. Noriko Kagemori and Dr. Satoshi Kimura, for their technical supports to the experiment in this study.

References

1) T.E. TIMELL: "Compression Wood in Gymnosperms 2", Springer-Verlag, Berlin Heidelberg, p. 1090 (1986).
2) A.J. STAMM: "Wood and Cellulose Science", The Ronald Press Company, New York, p. 218–227 (1964).
3) S. KAJITA: "Mokuzai-Kogaku", Yoken-do, Tokyo, p. 168 (1961).
4) A.J. PANSHIN and C. DE ZEEUW: "Textbook of Wood Technology, Vol. 1, Second Edition", McGraw-Hill Book Company, New York, p. 174–175 (1964).
5) E. MORK: *Papier Fabrikant*, **26**, 741–747 (1928).
6) W.A. COTE JR.: "Cellular Ultrastructure of Woody Plants", Syracuse University Press, New York, p. 392 (1965).
7) M. YUMOTO, S. ISHIDA and K. FUKAZAWA: *Res. Bull. College Exp. For. Hokkaido Univ.*, **40**(2), 409–454 (1983).
8) M. YUMOTO, S. ISHIDA and K. FUKAZAWA: *J. Fac. Agr. Hokkaido Univ.*, **60**(4), 312–335 (1982).
9) M. NORIMOTO, F. TANAKA, T. OHGAMA and R. IKIMUNE: *Wood Res. Tech. Notes.*, No. 22, 53–65 (1986).
10) R.A. COCKRELL: *Trans. Amer. Soc. Mech. Engrs.*, **69**, 931 (1947).
11) N.F. BARBER and B.A. MEYLAN: *Holzforschung*, **18**(5), 146–156 (1964).
12) N.F. BARBER: *Holzforschung*, **22**(4), 97–103 (1968).
13) I.D. CAVE: *Wood Sci. Technol*, **6**, 284–292 (1972).
14) R.E. PENTONEY: *J. For. Prod. Res. Soc.*, **3**(2), 27–32 (1953).
15) K. NAKATO and S. KAJITA: *J. Jpn. For. Soc.*, **37**(1), 22–25 (1955).
16) K. NAKATO: *Mokuzai Gakkaishi*, **4**(4), 134–141 (1958).
17) J.B. BOUTELJE: *Svensk Papperstidn.*, **65**, 209–215 (1962).
18) H.H. BOSSHARD: *Holz Roh- Werkstoff*, **14**(8), 285–295 (1956).
19) M. FUJITA and M. NORIMOTO: "Analysis of Anisotropic Periodicity for Cell Arrangement and Microfibril Orientation by the Various Diffraction Methods", Report of a Grand-in-Aid for Scientific Research (01480076) from The Ministry of Education, Science and Culture (1991).
20) A. ADACHI, Y. ISHIMARU, M. FUJITA and T. SADOH: *Mokuzai Gakkaishi*, **35**(8), 689–695 (1989).
21) T. MAEKAWA, M. FUJITA and H. SAIKI: *J. Soc. Mater. Sci. Jpn.*, **42**(473), 126–131 (1993).
22) T. YUHARA, M. HASUIKE and K. MURAKAMI: *Japan Tappi Journal*, **41**(6), 523–529 (1987).
23) A.J. STAMM: *Ind. Eng. Chem.*, **27**(4), 401–406 (1935).
24) S.C. CHAFE and J. ILIC: *Wood Sci. Technol.*, **26**, 181–187 (1992).
25) J.B. BOUTELJE: *Holzforschung*, **16**(2), 33–46 (1962).
26) H. YANO and T. YAMADA: *Mokuzai Gakkaishi*, **31**(3), 222–230 (1985).
27) L.J. GIBSON and M.F. ASHBY: "Cellular Solids", Pergamon Press, Oxford, p. 69–119(1988).
28) M. NORIMOTO, S. HAYASHI and T. YAMADA: *Holzforschung*, **32**(5), 167–172 (1978).
29) A.P. SCHNIEWIND: "Theory and Design of Wood and Fiber Composite Materials (B.A. Jayne ed.)", Syracuse University Press, New York, p. 83–95 (1972).
30) P.C. CHOU, J. CARLEONE and C.M. HSU: *J. Comp. Mater.*, **6**, 80–93 (1972).
31) R.C. TANG and N.N. HSU: *Wood and Fiber*, **5**, 139–151 (1973).
32) T. OHGAMA and M. NORIMOTO: *Bull. Fac. Edu., Chiba Univ.*, **33**, 127–145 (1984).
33) R.M. JONES: "Mechanics of Composite Materials (International student edition)", McGraw-Hill Kogakusha, Tokyo, p. 147–237 (1975).